

## **Robust 4D climate-optimal aircraft trajectory planning under weather-induced uncertainties**

### **Free-routing airspace**

Simorgh, Abolfazl; Soler, Manuel; Dietmüller, Simone; Matthes, Sigrun; Yamashita, Hiroshi; Castino, Federica; Yin, Feijia

#### **DOI**

[10.1016/j.trd.2024.104196](https://doi.org/10.1016/j.trd.2024.104196)

#### **Publication date**

2024

#### **Document Version**

Final published version

#### **Published in**

Transportation Research Part D: Transport and Environment

#### **Citation (APA)**

Simorgh, A., Soler, M., Dietmüller, S., Matthes, S., Yamashita, H., Castino, F., & Yin, F. (2024). Robust 4D climate-optimal aircraft trajectory planning under weather-induced uncertainties: Free-routing airspace. *Transportation Research Part D: Transport and Environment*, 131, Article 104196. <https://doi.org/10.1016/j.trd.2024.104196>

#### **Important note**

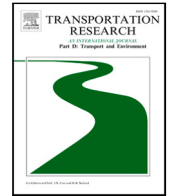
To cite this publication, please use the final published version (if applicable). Please check the document version above.

#### **Copyright**

Other than for strictly personal use, it is not permitted to download, forward or distribute the text or part of it, without the consent of the author(s) and/or copyright holder(s), unless the work is under an open content license such as Creative Commons.

#### **Takedown policy**

Please contact us and provide details if you believe this document breaches copyrights. We will remove access to the work immediately and investigate your claim.



# Robust 4D climate-optimal aircraft trajectory planning under weather-induced uncertainties: Free-routing airspace

Abolfazl Simorgh<sup>a,\*</sup>, Manuel Soler<sup>a</sup>, Simone Dietmüller<sup>b</sup>, Sigrun Matthes<sup>b</sup>, Hiroshi Yamashita<sup>b</sup>, Federica Castino<sup>c</sup>, Feijia Yin<sup>c</sup>

<sup>a</sup> Department of Aerospace Engineering, Universidad Carlos III de Madrid, 28911, Leganés, Spain

<sup>b</sup> Deutsches Zentrum für Luft- und Raumfahrt, Institut für Physik der Atmosphäre, Oberpfaffenhofen, Germany

<sup>c</sup> Faculty of Aerospace Engineering, Delft University of Technology, Delft, The Netherlands

## ARTICLE INFO

### Keywords:

Climate change  
Aircraft trajectory optimization  
Non-CO<sub>2</sub> climate-sensitive areas  
Meteorological uncertainty  
Robustness  
Robust optimal control

## ABSTRACT

The non-CO<sub>2</sub> climate impact of aviation strongly relies on the atmospheric conditions at the time and location of emissions. Therefore, it is possible to mitigate their associated climate impact by planning trajectories to re-route airspace areas with significant climate effects. Identifying such climate-sensitive regions requires specific weather variables. Inevitably uncertain weather forecasts can lead to inefficient aircraft trajectories if not accounted for within flight planning. The current study addresses the problem of generating robust climate-friendly flight plans under meteorological uncertainty characterized using the ensemble prediction system. We introduce a framework based on the concept of robust tracking optimal control theory to formulate and solve the proposed flight planning problem. Meteorological uncertainty effects on aircraft performance variables are captured using the formulated ensemble aircraft dynamical model and controlled by penalizing the performance index variance. Case studies show that the proposed approach can generate climate-optimized trajectories with minimal sensitivity to weather uncertainty.

## 1. Introduction

Carbon dioxide (CO<sub>2</sub>) and non-CO<sub>2</sub> aviation emissions contribute considerably to global warming (Lee et al., 2009). The most important non-CO<sub>2</sub> climate effects include the emissions of nitrogen oxides (NO<sub>x</sub>) (leading to changes in the concentration of ozone (O<sub>3</sub>) and methane (CH<sub>4</sub>)), water vapor (H<sub>2</sub>O), and persistent contrails (Lee et al., 2009; Brasseur et al., 2016). Despite the impacts of the COVID-19 pandemic on the aviation industry during the recent two years, which caused, at European level, declination of 55% and 44% of flight movements in 2020 and 2021, respectively, compared to 2019 (EUROCONTROL, 2022), it is estimated that the aviation industry will completely recover by 2024 (105% of 2019 at European level) (International Air Transport Association (IATA), 2022) and continue to grow by 1.2% annually. This will require the daily accommodation of 43.7 thousand flights (most-likely scenario) by 2050, which is 44% higher than in 2019 (EUROCONTROL, 2022). Such a growth rate of air traffic, in addition to critical operational-related issues such as capacity, efficiency, and safety, will significantly impact the environment within the current air traffic management (ATM) system. In fact, it is estimated that global aviation contributes approximately 3%–5% to the net anthropogenic effective radiative forcing (Lee et al., 2021). However, by accounting for the growth rate of the global air transport industry, the contribution is estimated to increase critically, and developing eco-efficient

\* Corresponding author.

E-mail address: [asimorgh@pa.uc3m.es](mailto:asimorgh@pa.uc3m.es) (A. Simorgh).

<https://doi.org/10.1016/j.trd.2024.104196>

Received 31 July 2023; Received in revised form 22 March 2024; Accepted 2 April 2024

Available online 6 May 2024

1361-9209/© 2024 The Author(s). Published by Elsevier Ltd. This is an open access article under the CC BY-NC license (<http://creativecommons.org/licenses/by-nc/4.0/>).

aviation is increasingly demanded. Addressing the climate impact of CO<sub>2</sub> emissions necessitates the development of more efficient aircraft and the use of alternative fuels or propulsion. However, the climate effects of non-CO<sub>2</sub> species, which are claimed to be responsible for approximately 66% of aviation's effective radiative forcing (Lee et al., 2010, 2021), have high spatial and temporal dependencies (e.g., see Simorgh et al., 2022b). Thus, by incorporating information about the altitude, location, and time dependencies of non-CO<sub>2</sub> climate effects in aircraft path planning, there is a possibility to reduce the overall climate effects induced by aviation.

To reduce the climate effects of non-CO<sub>2</sub> species within aircraft trajectory planning, we first require information on regions sensitive to aircraft emissions in terms of climate change, called climate-sensitive areas. The literature proposes a wide variety of approaches that directly or indirectly consider aviation-induced climate effects within aircraft trajectory planning, including reducing emissions (Celis et al., 2014), avoiding persistent contrail formation areas (Sridhar et al., 2011), reducing radiative forcing (Lim et al., 2017), and reducing global warming potential (Soler et al., 2014) (see Simorgh et al. (2022b)). One of the state-of-the-art approaches to modeling the climate impact of non-CO<sub>2</sub> emissions is toward using the prototype algorithmic climate change (aCCFs) functions which were initially introduced within the EU-project ATM4E (Matthes et al., 2017; Yamashita et al., 2021) and improved within the EU-project FlyATM4E (Matthes et al., 2023; Dietmüller et al., 2023; Yin et al., 2023). These aCCFs quantify the climate effects of NO<sub>x</sub> emissions, water vapor emissions, and persistent contrails by taking specific meteorological variables as inputs computationally fast; thus, they are suitable to be employed by aircraft trajectory optimization techniques. Recently, an open-source Python library (called CLIMaCCF) has been developed, implementing the latest version of aCCFs<sup>1</sup>. It is worth mentioning that the other state-of-the-art approach is the Contrail Cirrus Prediction Model (CoCiP), which is used to quantify the climate effects of contrails (Schumann, 2012). An open-source Python library, called pycontrails<sup>2</sup>, has been recently released, implementing the Lagrangian version of the CoCiP model, as well as the domain-filling version of CoCiP ("gridded" CoCiP: (Shapiro et al., 2022)). Interested readers are referred to Section 5.4 for a discussion on the differences between aCCFs and the "gridded" CoCiP model. Once information on the climate effects of aircraft emissions is obtained, it needs to be incorporated into flight planning tools to determine climate-friendly routes, i.e., aircraft trajectories with minimal impact on climate change. Numerous optimization methods have been suggested to find climate-friendly aircraft trajectories (see Simorgh et al. (2022b) for a classification of these techniques). These methods are direct (Lührs et al., 2016; Niklaßet al., 2017; Hartjes et al., 2016; Lührs et al., 2021) and indirect (Sridhar et al., 2011) optimal control approaches, genetic algorithm (Yamashita et al., 2020, 2021), mathematical programming (Campbell et al., 2008), and path-finding algorithms (Rosenow et al., 2017). The optimization criteria defined in these studies are typically a weighted sum of objectives that directly or indirectly represent operating cost (e.g., fuel and/or time) and climate effects (e.g., avoidance of forming persistent contrails), respectively. Such objectives generally behave in a conflicting manner, and a suitable selection of weights needs to be made to determine Pareto-optimal solutions (Castino et al., 2023).

In order to calculate aCCFs of non-CO<sub>2</sub> species (or also using CoCiP for contrails), weather variables, such as temperature and relative humidity, are needed. In addition, the components of wind and temperature are required to calculate the trajectory and performance variables of the aircraft. As the required meteorological variables for climate-optimal trajectory planning are obtained from inevitably uncertain weather forecasts, the flight planning procedure to mitigate climate impact is associated with uncertainty. It should be noted that due to reliance on more meteorological variables, the sensitivity of flight planning with objectives related to climate effects is higher than business-as-usual ones. The presence of uncertainty in calculating aCCFs and the aircraft dynamical model, if not considered, can lead to inefficient flight planning. It is worth mentioning that meteorology is not the only source of uncertainty affecting climate-optimal trajectories' efficiency. In fact, the current level of scientific understanding of aviation-induced climate impact is relatively immature. According to Lee et al. (2021), unlike the climate impact induced by CO<sub>2</sub> emissions, which is estimated with high certainty, the confidence level (characterized based on evidence and agreement) for estimating the effective radiative forcing of the non-CO<sub>2</sub> species is medium or low. For instance, the impact of water vapor emissions is estimated with medium uncertainty, while the confidence levels for contrail cirrus and net NO<sub>x</sub>-induced climate effects are low. Therefore, climate science acts as an additional source of uncertainties. However, considering meteorological uncertainty is more straightforward and reasonable as a preliminary step toward increasing the reliability and efficiency of such climate-friendly flight planning. In this respect, reliable weather forecasts capable of representing possible deviations in weather conditions are required. Currently, the ensemble prediction system (EPS) is known as a promising approach to characterizing uncertainty in weather variables by generating  $N_{\text{EPS}}$  individual forecasts (Bauer et al., 2015). Each forecast (called an ensemble member) indicates a possible realization of weather variables.

A vast majority of studies proposed to mitigate the non-CO<sub>2</sub> climate effects consider them to be deterministic (see Simorgh et al. (2022b)). Only a few very recent studies (Baneshi et al., 2023; Simorgh et al., 2022, 2023) have started to look at how to integrate meteorological uncertainty, which can be typically characterized using EPS, to determine robust climate-optimal trajectories. In Baneshi et al. (2023), a deterministic aircraft trajectory optimization problem with constant flight altitude is solved by considering the ensemble mean (i.e., taking the average from all ensemble members) to represent meteorology, and then the effects of all possible realizations of weather variables are reflected in the flight performance variables, including flight time, fuel burn and climate effects using an ensemble trajectory prediction. This study (i.e., Baneshi et al. (2023)), however, mainly quantifies the effects of uncertainty associated with different members rather than optimizing. More sophisticated methods, including all ensemble members in the trajectory optimization, have been proposed by Simorgh et al. (2022, 2023). In Simorgh et al. (2022), an EPS-based

<sup>1</sup> CLIMaCCF library can be accessed using DOI: 10.5281/zenodo.6977272

<sup>2</sup> pycontrails library can be accessed using DOI: 10.5281/zenodo.7877538

robust aircraft trajectory planning method was proposed to mitigate climate effects within free-routing airspace. The aCCFs are employed to model the climate effects, and the optimization is performed using the direct optimal control approach. However, the focus of Simorgh et al. (2022) was restricted only to optimizing the lateral path, and the potential to mitigate climate effects by changing the flight altitude was ignored. The joint optimization of altitude profile and aircraft speed profile, in addition to the lateral path, has been addressed by Simorgh et al. (2023) for the currently structured airspace using the Augmented Random Search algorithm. One of the steps planned toward enhancing the efficiency of the current ATM system is the transition from structured airspace to a free-routing one (considered in phase B of the European ATM master plan (Single European Sky ATM Research Joint Undertaking (SESAR JU), 2020)). The method proposed by Simorgh et al. (2023) is not suitable for the context of fully free-routing airspace. To our knowledge, the full 4D climate-optimized aircraft trajectory planning problem under meteorological uncertainty has yet to be explored in the literature (see Table 1).

This study, therefore, aims to address, for the first time, the problem of full 4D robust climate-optimal flight planning within the context of free-routing airspace. The meteorological uncertainty is characterized by employing the EPS weather forecast, and the aviation-induced climate effects are quantified using the latest version of aCCFs (aCCF V1.0 A (Matthes et al., 2023)). Our focus is restricted to aCCFs as they assess the climate impact of the most important non-CO<sub>2</sub> species (e.g., NO<sub>x</sub>-induced ozone and methane, and contrails) in the same unit, i.e., Kelvin. With robustness, we refer to trajectories with minimal sensitivity to meteorological uncertainty while satisfying user-defined objectives and being operationally feasible. It is important to note that the aim of trajectory optimization is to deliver a unique (i.e., deterministic) flight plan that is optimized considering the performance associated with all ensemble members. This is one of the main reasons that deterministic approaches in the literature are not efficient for flight planning under uncertainty effects. For instance, in the case of using an ensemble weather forecast, performing  $N_{\text{EPS}}$  (number of ensemble members) deterministic trajectory optimizations for each ensemble member independently will result in  $N_{\text{EPS}}$  optimized flight plans, each exhibiting optimal performance under the corresponding weather scenario and not necessarily the other ensemble members. As the realization of the uncertainty is not known before committing to a specific plan, the decision to use one of the optimized trajectories cannot be effectively made. Thus, there is a need to determine a deterministic flight plan that performs robustly to the considered potential deviations in the forecasted meteorological conditions. To address this optimization problem, we propose a robust tracking optimal control framework to model the EPS-based climate-optimal flight planning problem. Considering the fact that the robust optimal control problem formulated using EPS weather forecasts to quantify uncertainty has a finite representation (associated with the ensemble members), we convert the robust optimization formulations to a deterministic problem with a larger dimension. Unlike the studies conducted by Simorgh et al. (2022, 2023), which considered only average performance as the objective, we define the objective function in a manner that allows also controlling the uncertainty ranges of the considered objectives, e.g., estimated climate effects. Based on the proposed methodology in this study, we have developed an open-source Python library called ROC (Robust Optimal Control for flight planning). The ROC library is publicly available and can be accessed using the DOI: <https://doi.org/10.5281/zenodo.10552812>.

The subsequent sections of the paper are structured as follows. We state the aircraft trajectory optimization problem with climate impact as the flight planning objective in Section 2. Section 3 presents the robust tracking optimal control framework used to formulate the proposed robust flight planning problem, which is stated in Section 4. The effectiveness of our methodology to mitigate aviation-induced climate effects is explored in Section 5, and Section 6 closes the paper with some concluding remarks.

## 2. Climate-optimized aircraft trajectory planning

The aviation-induced non-CO<sub>2</sub> climate effects depend highly on the geographic location, altitude, and time of emissions. In light of this, determining aircraft routes that can potentially reduce emissions in regions highly sensitive to climate change is a step toward climatically efficient air transport. Achieving this goal requires acquiring information about climate-sensitive areas as a primary step. Once such climate impact information is available, it must be integrated into flight planning tools to generate climate-aware flight paths. It needs to be highlighted that ensuring reliable trajectories involves identifying, comprehending, and quantifying different sources of uncertainty (Matthes et al., 2023; Simorgh et al., 2022b).

In this study, we employ aCCFs-V1.0 A (Matthes et al., 2023) to quantify aviation-induced climate effects and consider meteorological uncertainty quantified using EPS to generate robust climate-optimal trajectories. In the following, we present the elements required to state the robust climate-optimal flight planning problem, i.e., aCCFs, aircraft dynamical model, and meteorological uncertainty (which perturbs the aircraft dynamical model and the estimated climate effects). In the last part of this section, the cost function of the flight planning problem is presented.

### 2.1. Aviation-induced climate effects quantified using aCCFs

To plan climate-optimal trajectories, spatio-temporally resolved information on aviation-induced climate effects is required. In this study, we rely on the so-called aCCFs to estimate the climate impact induced by aircraft emissions. The main reasons for using aCCFs to identify climate-sensitive areas in this study are as follows: (1) aCCFs are computationally compatible with aircraft trajectory optimization tools as they can be calculated in real-time, (2) aCCFs estimate climate impact directly in temperature change, and (3) aCCFs account for the temporal and spatial dependencies of climate effects corresponding to the most relevant non-CO<sub>2</sub> species, e.g., ozone and methane, water vapor emissions, and persistent contrails. We use the prototype aCCFs according to the latest published findings of the EU-Project FlyATM4E (Yin et al., 2023; Dietmüller et al., 2023; Matthes et al., 2023), which include the aCCFs for CO<sub>2</sub> and non-CO<sub>2</sub> effects, i.e., the effects of ozone and methane induced by NO<sub>x</sub> emissions, the effects of water vapor,

**Table 1**

A classification of the most recent studies (i.e., from 2018) conducted on aircraft trajectory optimization w.r.t. climate impact.

Study	Degrees of freedom			Considered factors		Flight planning	
	Lateral route	Flight altitude	Speed	Climate effects	MET uncertainty	Routing	Methodology
Yin et al. (2018a)	✓	✓		NO <sub>x</sub>		Free-routing	Genetic algorithm
Yin et al. (2018b)	✓	✓		Contrails (potential contrail coverage)		Free-routing	Genetic algorithm
Niklaß et al. (2021)	✓	✓	✓	AIC, O <sub>3</sub> , CH <sub>4</sub> , H <sub>2</sub> O, CO <sub>2</sub>		Free-routing	Direct optimal control
Yamashita et al. (2020) Yamashita et al. (2021) Yin et al. (2023) Castino et al. (2021)	✓	✓		AIC, O <sub>3</sub> , CH <sub>4</sub> , H <sub>2</sub> O, CO <sub>2</sub>		Free-routing	Genetic algorithm
Vitali et al. (2021)	✓	✓	✓	AIC, O <sub>3</sub> , CH <sub>4</sub> , H <sub>2</sub> O, CO <sub>2</sub>		Free-routing	Direct optimal control
Matthes et al. (2020) Lührs et al. (2021)	✓	✓	✓	AIC, O <sub>3</sub> , CH <sub>4</sub> , H <sub>2</sub> O, CO <sub>2</sub>		Free-routing	Direct optimal control
Baneshi et al. (2023)	✓		✓	AIC, O <sub>3</sub> , CH <sub>4</sub> , H <sub>2</sub> O, CO <sub>2</sub>	Trajectory prediction	Free-routing	Direct optimal control
Simorgh et al. (2022)	✓		✓	AIC, O <sub>3</sub> , CH <sub>4</sub> , H <sub>2</sub> O, CO <sub>2</sub>	✓	Free-routing	Direct optimal control
Simorgh et al. (2023)	✓	✓	✓	AIC, O <sub>3</sub> , CH <sub>4</sub> , H <sub>2</sub> O, CO <sub>2</sub>	✓	Structured	Augmented random search
Current study	✓	✓	✓	AIC, O <sub>3</sub> , CH <sub>4</sub> , H <sub>2</sub> O, CO <sub>2</sub>	✓	Free-routing	Direct (robust) optimal control

and the effects of contrail-cirrus. The aCCFs can be calculated efficiently, as their mathematical formulation only needs input data of specific meteorological variables (e.g., temperature and geopotential). Calculated aCCFs quantify the global climate effect using the average temperature response (ATR20) as the climate indicator. A detailed description of the mathematical formulation of the aCCFs is given in Yin et al. (2023). In the following, general dependencies of the individual aCCFs to meteorological variables are shortly shown:

$$\begin{aligned}
 \text{aCCF}_{\text{NO}_x} &= \text{aCCF}_{\text{O}_3} + \text{aCCF}_{\text{CH}_4} + \text{aCCF}_{\text{PMO}} && [\text{K/Kg}(\text{NO}_2)] \\
 \text{aCCF}_{\text{O}_3} &= f_{\text{O}_3}(T, \Phi) && [\text{K/Kg}(\text{NO}_2)] \\
 \text{aCCF}_{\text{CH}_4} &= f_{\text{CH}_4}(F_{in}, \Phi) && [\text{K/Kg}(\text{NO}_2)] \\
 \text{aCCF}_{\text{PMO}} &= f_{\text{PMO}}(F_{in}, \Phi) && [\text{K/Kg}(\text{NO}_2)] \\
 \text{aCCF}_{\text{H}_2\text{O}} &= f_{\text{H}_2\text{O}}(PV) && [\text{K/Kg}(\text{fuel})] \\
 \text{aCCF}_{\text{dCont.}} &= f_{\text{dCont.}}(OLR), && [\text{K/km}(\text{contrails})] \\
 \text{aCCF}_{\text{nCont.}} &= f_{\text{nCont.}}(T), && [\text{K/km}(\text{contrails})]
 \end{aligned} \tag{1}$$

where  $T$  is the temperature,  $\Phi$  is the geopotential,  $F_{in}$  is the incoming solar radiation at the top of the atmosphere,  $PV$  is the potential vorticity, and  $OLR$  is the outgoing longwave radiation. The aCCFs of contrails (i.e., day-time and night-time) are only calculated for areas where persistent contrails are generated, called persistent contrails formation areas (PCFAs). For these PCFAs, two meteorological conditions are needed: the Schmidt-Appleman criterion (Appleman, 1953) has to be fulfilled, and moreover, the atmosphere has to be ice-supersaturated. The aCCF of CO<sub>2</sub> emissions is independent of the atmospheric location at the time of emissions, i.e.,  $\text{aCCF}_{\text{CO}_2} = \text{constant}$  [K/Kg(fuel)]. Interested readers are referred to Yin et al. (2023) for the mathematical functions  $f_i$  for  $i \in \{\text{O}_3, \text{CH}_4, \text{PMO}, \text{H}_2\text{O}, \text{dCont.}, \text{nCont.}\}$ . As can be understood from the specific units of aCCFs, fuel flow, NO<sub>x</sub> emission index, and the flown distance in PCFAs are required to quantify the climate effects in Kelvin.

The study conducted by Yin et al. (2023) introduces the first consistent set of aCCFs (named aCCF-V1.0). The mathematical formulations of aCCF-V1.0 are given using ATR integrated over the next 20 years for a pulse emission (P-ATR20). In order to make the aCCFs well-suited for the purpose of our mitigation study, some additional assumptions were taken, which are described in the following. We use aCCF version 1.0 A, where aCCFs are calibrated to the results of the state-of-the-art climate response model AirClim (Dahlmann et al., 2016), aiming at addressing uncertainty due to the current state of scientific knowledge of climate impacts (the calibration factors are introduced in Matthes et al. (2023)). We also apply so-called metric conversion factors (reported in Table 5 of Dietmüller et al. (2023)) in order to convert from P-ATR20 to F-ATR20, with F-ATR20 using the future business-as-usual

emission scenario. In fact, with the future emission scenario, we want to measure the climate impact of steadily using a specific routing option, enabling us to quantify the mitigation potential of that routing option employed by air traffic operations. Moreover, we consider the efficacies of individual climate effects, as some non-CO<sub>2</sub> species can be less or more effective in changing the global mean temperature than CO<sub>2</sub>. Here, we use the efficacy factors summarized by Lee et al. (2021).

## 2.2. Aircraft dynamical model

In order to generate efficient aircraft trajectories, we rely on dynamical models that can provide an acceptable estimation of aircraft behavior in practice while being computationally inexpensive. To this end, we utilize the three-degrees-of-freedom point mass model, having the following equations of motion (González-Arribas et al., 2023):

$$\frac{d}{dt} \begin{bmatrix} \phi \\ \lambda \\ h \\ v_{tas} \\ m \end{bmatrix} = \begin{bmatrix} (v_{tas} \cos(\gamma) \cos(\chi) + w_y)(R_M(\phi) + h)^{-1} \\ (v_{tas} \cos(\gamma) \sin(\chi) + w_x) \left( (R_N(\phi) + h) \cos(\phi) \right)^{-1} \\ v_{tas} \sin(\gamma) \\ (T(C_T) - D(C_L))m^{-1} - g \sin(\gamma) \\ -f_c(C_T) \end{bmatrix} \quad \begin{array}{l} \text{Latitude, Longitude : } \phi, \lambda \\ \text{Altitude, True airspeed : } h, v_{tas} \\ \text{Mass, Fuel flow : } m, f_c \\ \text{Thrust \& Drag forces : } T, D \\ \text{Thrust \& Lift coefficients : } C_T, C_L \\ \text{Components of wind : } w_x, w_y \\ \text{Heading \& Path angles : } \chi, \gamma \end{array} \quad (2)$$

where  $C_L(\gamma) = (2mg \cos(\gamma)) / (\rho v_{tas}^2 S)$ ,  $g$  is the gravitational acceleration,  $S$  is the wetted wing surface,  $\rho$  is the air density,  $R_M$  and  $R_N$  are the radii of curvature of the meridian's ellipse and the radius of curvature in the prime vertical, respectively. BADA4.2 is used to represent the aircraft's aerodynamic and propulsive performance (Gallo et al., 2006). A feasible aircraft trajectory needs to fulfill a set of constraints representing the flight envelope. Particularly, the limitations imposed for calibrated airspeed, thrust and lift coefficients, Mach, and altitude are given in the following:

$$\begin{aligned} v_{CAS, stall} &\leq v_{CAS}(v) \leq v_{CAS, max} \\ C_{T, min} &\leq C_T \leq C_{T, max} \\ M(v_{tas}) &\leq M_{max} \\ C_L &\leq C_{L, max} \\ h &\leq h_{max} \end{aligned} \quad (3)$$

where  $M$  is the Mach number and  $v_{CAS}$  is the calibrated airspeed.

## 2.3. Meteorological uncertainty

We rely on standard weather forecasts that provide a prediction of the status of atmospheric variables, such as wind and temperature, required for flight planning. Due to many factors, such as limited knowledge about the state of the atmosphere, and computational constraints, weather forecasts are unavoidably uncertain. Such uncertainty can seriously affect ATM performance. In order to assess the non-CO<sub>2</sub> climate effects using aCCFs, additional meteorological variables are required (e.g., potential vorticity and temperature). This implies that the sensitivity of climate-optimal flight planning to meteorological uncertainty is higher than the business-as-usual (or cost-optimal) one.

The main state-of-the-art framework in the meteorological community is the ensemble prediction system (EPS)-based weather forecasting, which generates  $N_{EPS}$  predictions (so-called ensemble members) by systematically slightly perturbing the initial state of the atmosphere or/and parameters of a numerical weather integration model. In this study, we use the ECMWF ERA5 reanalysis ensemble data product (which includes ten ensemble members) (Hersbach et al., 2020). Fig. 1 shows the geographical distribution at 225 hPa of temperature and relative humidity over ice, and from these two variables, the calculated PCFAs for two different ensemble members. Comparing the two different ensembles, we conclude that the variability in the PCFAs is rather high due to the high variability in the relative humidity field. In the last row of Fig. 1, three different routes are illustrated. We see that the cost-optimal trajectory flies through PCFAs for both ensemble members. If one uses the first ensemble member to plan a contrails-optimal trajectory and the second ensemble member is more representative of the actual weather conditions, the planned route will be inefficient. This is because, besides not mitigating climate impact, it increases the operating cost due to flying longer routes. However, it is possible to determine a trajectory with lower sensitivity to meteorological uncertainty during the planning stage if information on potential weather conditions is available. For instance, the trajectory with the dark-blue color has a robust performance for the two given forecasts. In this study, we aim to use the information provided by an EPS weather forecast to plan climate-optimized routes with robust performance to meteorological uncertainty. It is worth mentioning that including such information in flight planning is not straightforward and adds complexity to the optimization problem in which, instead of using one forecast and solving a deterministic optimization, we need to consider  $N_{EPS}$  probable forecasts. In addition, solving  $N_{EPS}$  deterministic optimization problems, each considering one forecast, is not operationally feasible and efficient, as the information on the uncertainty's realization is unavailable before committing to a specific plan. In this study, we formulate the aircraft trajectory problem considering all ensemble members in an operationally feasible and efficient manner.

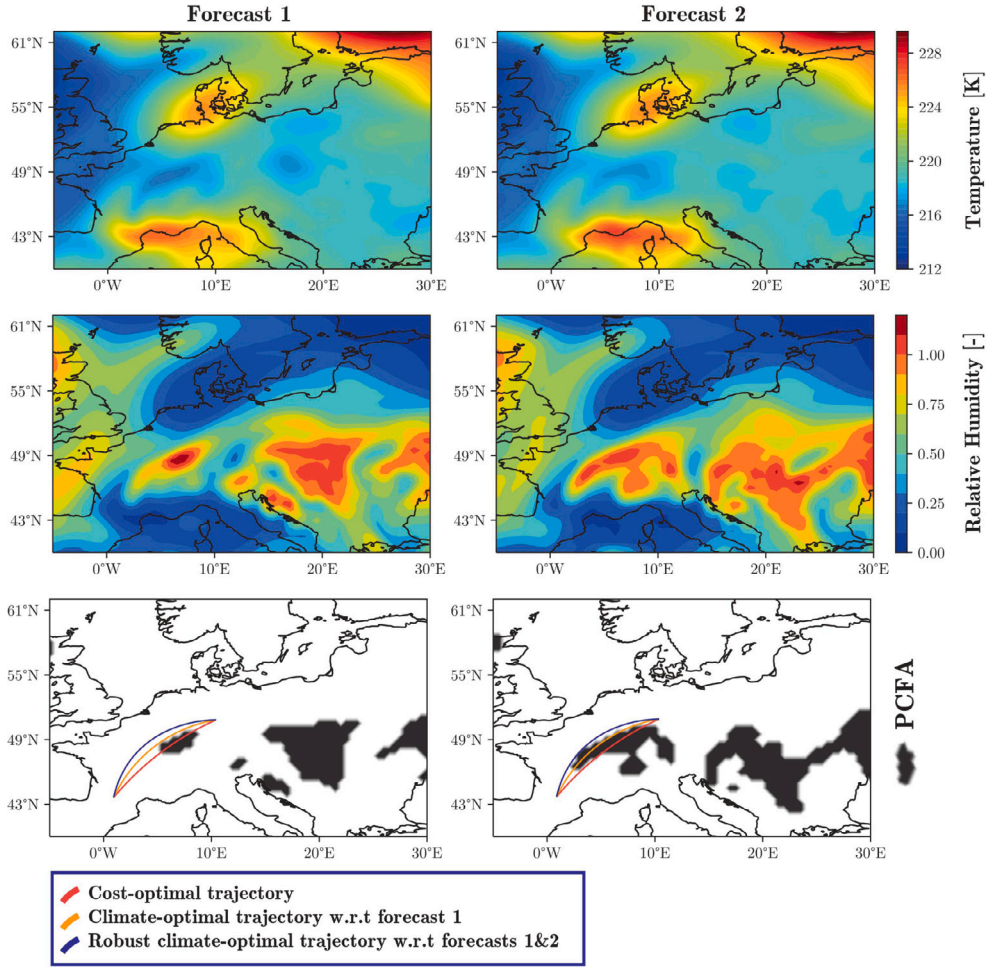


Fig. 1. Meteorological variables required to calculate PCFAs and identified PCFAs for two different ensemble members (i.e., two different members of an EPS weather forecast) at 225 hPa on June 13, 2018, 0000 UTC. (For interpretation of the references to color in this figure legend, the reader is referred to the web version of this article.)

#### 2.4. Objective function modeling

To determine climate-optimal trajectories, climate-sensitive regions need to be considered and penalized in the objective function of the trajectory optimization problem. As presented in Section 2.1, we employ aCCFs V1.0 A for quantifying climate effects. In addition to the climate impacts, fuel burn and flight time are crucial factors that are usually considered as objectives to be optimized. Due to the existence of uncertainty in the considered objectives (i.e., effects of meteorological uncertainty), the objective function is to be defined such that a robust trajectory is determined under weather uncertainty. To this end, we define the following performance index:

$J = \text{Simple Operating Cost} + \text{Average temperature response}$

$$\text{Simple Operating Cost} : \text{CI}_m \cdot \mathbb{E}\{\text{SOC}\} + \text{CI}_{dp} \cdot \mathbb{V}\{\text{SOC}\} \quad (4)$$

$$\text{Average temperature response} : \text{EI}_m \cdot 10^{10} \cdot \mathbb{E}\{\text{ATR}\} + \text{EI}_{dp} \cdot 10^{15} \cdot \mathbb{V}\{\text{ATR}\}$$

where

$$\text{SOC} := \left[ C_t \cdot [t_f - t_0] + C_f \cdot [m(t_0) - m(t_f)] \right]$$

$$\text{ATR} := \int_{t_0}^{t_f} \sum_{i=1}^5 \text{ATR}_i(t, \mathbf{x}(t), \mathbf{u}(t)) dt \quad (5)$$

for  $i \in \{\text{CH}_4, \text{Cont.}, \text{O}_3, \text{H}_2\text{O}, \text{CO}_2\}$  as

$$\begin{aligned} \text{ATR}_{\text{CH}_4}(t, \mathbf{x}) &= 10^{-3} \times \text{aCCF}_{\text{CH}_4}(t, \mathbf{x}) \cdot \dot{m}_{\text{nox}}(t) \\ \text{ATR}_{\text{O}_3}(t, \mathbf{x}) &= 10^{-3} \times \text{aCCF}_{\text{O}_3}(t, \mathbf{x}) \cdot \dot{m}_{\text{nox}}(t) \\ \text{ATR}_{\text{Cont.}}(t, \mathbf{x}) &= 10^{-3} \times \text{aCCF}_{\text{Cont.}}(t, \mathbf{x}) \cdot v_{gs}(t) \\ \text{ATR}_{\text{H}_2\text{O}}(t, \mathbf{x}) &= -\text{aCCF}_{\text{H}_2\text{O}}(t, \mathbf{x}) \cdot \dot{m}(t) \\ \text{ATR}_{\text{CO}_2}(t, \mathbf{x}) &= -\text{aCCF}_{\text{CO}_2} \cdot \dot{m}(t) \end{aligned} \quad (6)$$

where  $\mathbf{x}$  is the state vector of the aircraft dynamical model, which includes the location of flight in the atmosphere (i.e.,  $\lambda$ ,  $\phi$ , and  $h$ ) and  $\dot{m}_{\text{nox}}(t) = f_c(C_T) \cdot \text{EI}_{\text{NO}_x}$ .  $\text{EI}_{\text{NO}_x}$  is the  $\text{NO}_x$  emission index estimated utilizing Boeing Fuel Flow Method 2 (DuBois and Paynter, 2006). Such a definition of objective function allows considering both cost and climate impact simultaneously as objectives to be minimized. However, a trade-off generally exists between these two objectives determined by the selection of cost and environmental indices, i.e., CI and EI, respectively. The parameters  $C_i$  and  $C_f$  determine the importance of flight time and fuel consumption in representing the operating cost.

Due to the uncertainty in the variables considered as objectives, the average (denoted with operator  $\mathbb{E}\{\cdot\}$ ) and variance (denoted with operator  $\mathbb{V}\{\cdot\}$ ) of SOC and ATR were considered in defining the objective function. The weights of the expected values and variances of objectives are denoted with subscripts 'm' and 'dp', respectively. Notice that the aim of using constant weights for the average and variance of ATR (i.e.,  $10^{10}$  and  $10^{15}$ , respectively) is to scale the order of climate effects with respect to SOC. It is important to highlight that we defined the objective function in the framework of optimal control theory, including both the Lagrange and Mayer terms, collectively referred to as Bolza (Betts, 2010).

### 3. Robust tracking optimal control problem

The optimal control theory is typically employed to formulate the aircraft trajectory optimization problem as it allows us to include realistic dynamical models of aircraft suitably, impose physical and operational constraints, and also define flight planning objectives (Simorgh et al., 2022b). Due to the inevitable presence of uncertainty in predicting atmospheric conditions and their effects on aircraft trajectories, we formulate the aircraft flight planning problem within the framework of robust optimal control theory. In the following, we state a general formulation of the robust optimal control problem together with a solution approach that will be used in Section 4 to solve our proposed robust climate-optimized trajectory planning problem.

#### 3.1. General formulation

Let us define  $\zeta$  as a vector containing uncertain variables of a dynamical system. The uncertainties are modeled as continuous random variables  $\zeta(\cdot) : \Delta \rightarrow \mathbb{R}^{n_\zeta}$ , where  $\Delta$  is a space of possible outcomes. For each possible outcome  $\delta \in \Delta$ , the random variable takes a specific value ( $\zeta(\delta)$ ). With such a representation of uncertainty, a general class of robust tracking optimal control problems is stated as follows (González-Arribas et al., 2018):

$$\min_{\mathbf{u}(t)} J = \mathbb{E} \left\{ M(t_0, t_f, \mathbf{x}(t_0), \mathbf{x}(t_f)) + \int_{t_0}^{t_f} L(\mathbf{x}(t, \delta), \mathbf{u}(t, \delta), \mathbf{z}(t, \delta), \zeta(\delta)) dt \right\} \quad (7)$$

$$\text{subject to : } \dot{\mathbf{x}}(t) = \mathbf{f}(\mathbf{x}(t, \delta), \mathbf{u}(t, \delta), \mathbf{z}(t, \delta), \zeta(\delta)), \quad \mathbf{x}(t_0) = \Psi_0(\zeta(\delta), t_0) \quad (8)$$

$$\mathbf{h}(\mathbf{x}(t, \delta), \mathbf{u}(t, \delta), \mathbf{z}(t, \delta), \zeta(\delta)) = \mathbf{0} \quad (9)$$

$$\mathbf{g}(\mathbf{x}(t, \delta), \mathbf{u}(t, \delta), \mathbf{z}(t, \delta), \zeta(\delta)) \leq \mathbf{0} \quad (10)$$

$$\mathbb{E}\{\Psi(t_0, t_f, \mathbf{x}(t_0), \mathbf{x}(t_f))\} = \mathbf{0} \quad (11)$$

$$T_x(\mathbf{x}(t, \delta_1) - \mathbf{x}(t, \delta_2)) = 0 \quad \forall \delta_1, \delta_2 \in \Delta \quad (12)$$

$$T_u(\mathbf{u}(t, \delta_1) - \mathbf{u}(t, \delta_2)) = 0 \quad \forall \delta_1, \delta_2 \in \Delta \quad (13)$$

$$T_z(\mathbf{z}(t, \delta_1) - \mathbf{z}(t, \delta_2)) = 0 \quad \forall \delta_1, \delta_2 \in \Delta \quad (14)$$

where  $\mathbf{x}(\cdot) \in \mathbb{R}^{n_x}$ ,  $\mathbf{u}(\cdot) \in \mathbb{R}^{n_u}$ , and  $\mathbf{z}(\cdot) \in \mathbb{R}^{n_z}$  are the vectors of states, controls, and algebraic variables, respectively. The equation (7) is a general form of the objective function considered for modeling optimal control problems under uncertainty effects, thus not specifically related to aircraft trajectory planning (González-Arribas et al., 2018). It consists of two nonlinear functions: Mayer (represents terminal cost) and Lagrange (represents the cost to go or running cost) terms (Kirk, 2004). The Mayer term is a nonlinear function that maps  $M : \mathbb{R} \times \mathbb{R} \times \mathbb{R}^{n_x} \times \mathbb{R}^{n_x} \rightarrow \mathbb{R}$ , is used for objectives that are evaluated at boundaries. In contrast, the objectives that are evaluated over the whole optimization interval are represented in the form of Lagrange, mapping  $L : \mathbb{R}^{n_x} \times \mathbb{R}^{n_u} \times \mathbb{R}^{n_z} \times \mathbb{R}^{n_\zeta} \times \mathbb{R} \rightarrow \mathbb{R}$ . For instance, as stated earlier (in Eq. (4)), to model the flight planning objective function in this study, the simple operating cost, which is a function of flight time and fuel consumption, is considered as the Mayer term as they are only evaluated at boundaries. However, the climate impact, which is evaluated at each point along the trajectory, is defined in the Lagrange form. In Eq. (7),  $\mathbb{E}\{\cdot\}$  denotes the expectation operator due to the uncertainties in the dynamical model (i.e., Eq. (8)). Notice that the performance index

is not limited to the expectation of objectives, and one can evaluate other statistics under the current formulation. As an example, the variance of a function  $Y(\delta)$  can be calculated as  $\mathbb{V}\{Y\} = \mathbb{E}\{(Y - \mathbb{E}\{Y\})^2\} = \mathbb{E}\{Y^2\} - \mathbb{E}\{Y\}^2$ .

The Eq. (8) represents a general class of nonlinear dynamical systems called tyochastic dynamical systems, where  $\mathbf{f}$  is a vector field that maps  $\mathbb{R}^{n_x} \times \mathbb{R}^{n_u} \times \mathbb{R}^{n_z} \times \mathbb{R}^{n_\zeta} \times \mathbb{R}^+ \rightarrow \mathbb{R}^{n_x}$ . This equation is called the state-space representation of a dynamical system, which is composed of a set of first-order (linear or nonlinear) differential equations that describe how the state variables ( $\mathbf{x}$ ) (e.g., atmospheric location of flight (latitude, longitude, and flight altitude), true airspeed, and aircraft mass) evolve over time ( $\dot{\mathbf{x}}$ ) in response to both the current state ( $\mathbf{x}$ ) and the system's inputs ( $\mathbf{u}$ ) (e.g., thrust, heading angle, flight path angle), and in some cases algebraic variables  $\mathbf{z}$  (e.g., ground speed) and uncertainty ( $\zeta$ ) (e.g., uncertainty in direction and speed of wind). The specific form of the function  $\mathbf{f}$  depends on the nature of the dynamical system and can be linear or nonlinear. In the context of flight planning, we refer to Eq. (8) as the dynamical model of aircraft, which is represented using the full 4D point-mass model given in Eq. (2). The vector fields  $\mathbf{h} : \mathbb{R}^{n_x} \times \mathbb{R}^{n_u} \times \mathbb{R}^{n_z} \times \mathbb{R}^{n_\zeta} \times \mathbb{R}^+ \rightarrow \mathbb{R}^{n_h}$  and  $\mathbf{g} : \mathbb{R}^{n_x} \times \mathbb{R}^{n_u} \times \mathbb{R}^{n_z} \times \mathbb{R}^{n_\zeta} \times \mathbb{R}^+ \rightarrow \mathbb{R}^{n_g}$  are the equality and inequality constraints, respectively, given in Eqs. (9),(10), with  $n_z \leq n_h$ . Finally, the function including the boundary conditions ( $\Psi : \mathbb{R} \times \mathbb{R} \times \mathbb{R}^{n_x} \times \mathbb{R}^{n_x} \rightarrow \mathbb{R}$ ) imposed in average is given in Eq. (11).  $\mathbf{0}$  is a vector of zeros with appropriate dimensions.

The equality conditions imposed in Eqs. (12)–(14) are suitable for those practical problems required to deliver unique trajectories for some state and control variables under uncertainty effects, i.e., such variables should be equal in all scenarios (i.e., for all realizations of uncertainties ( $\forall \delta_1, \delta_2 \in \Delta$ )). Such variables are called tracked, and the class of dynamical optimization problems with tracking conditions is called tracking robust optimal control. Here, with these sets of constraints, we are imposing the tracking conditions, i.e., the tracked variables should be equal in all scenarios (i.e., for all realization of uncertainties ( $\forall \delta_1, \delta_2 \in \Delta$ )). In Eqs. (12)–(14),  $T_x$ ,  $T_u$ , and  $T_z$  are matrices with appropriate dimensions projecting the state vector, control vector, and vector of algebraic variables into the tracked parts. It is worth mentioning that the tracking constraints are equality-type path constraints. However, they are presented separately to emphasize the tracking type of the robust optimal control problem.

The objective of the formulated robust optimal control problem is to determine a control policy  $\mathbf{u}(\cdot)$  (which is the decision vector of the optimization problem) such that a cost functional Eq. (7) gets minimized and the conditions Eqs. (8)–(14) are satisfied. An open-loop control policy (i.e.,  $\mathbf{u}(t)$ ) is inefficient for such a class of optimization problems. In fact, control inputs with dependency only on time transform all uncertainty effects into the states of the dynamical system (through the dynamical model). In this respect, the range of feasible solutions to satisfy tracking conditions is limited, or even, in many cases, a feasible solution cannot be found. One possibility is to use the scenario-dependent control scheme (i.e.,  $\mathbf{u}(t, \delta)$ ), in which, depending on each realization of uncertainty, the control input is applied to guarantee the uniqueness of tracking variables (i.e., satisfying tracking conditions). With this approach, a part of the uncertainty is considered on the control inputs. This strategy applies only to those systems with a low-level controller in practice to generate control policy to follow tracked states in real-time at a shorter timescale than the optimal control problem.

### 3.2. Solution approach: Discretization of robust optimal control problem

For each realization of uncertain parameters (i.e.,  $\zeta(\delta = \delta_0)$ ) in the formulated robust optimal control problem, one can find the optimal solution in a deterministic manner. In this respect, one possibility suggested in the literature is to approximate the uncertainty with a discrete distribution, leading to a finite representation of the robust optimal control problem (González-Arribas et al., 2018). In the following, we will briefly present how a robust optimal control problem formulation with a finite representation can be converted to a deterministic problem with a larger dimension (González-Arribas et al., 2018).

Let us consider a finite collection of the  $n$  discrete samples of uncertainty  $\{\zeta_i\}$  with the associated weights  $\{w_i\}$  ( $w_i \geq 0, \forall i$ ), satisfying  $\sum_{i=1}^n w_i = 1$ . Then, we construct the probability measure as:

$$\mathcal{P}(A) = \sum_{i=1}^n w_i \delta_{\zeta_i}(A) \quad (15)$$

where  $\delta_x(\cdot)$  denotes the Dirac measure, i.e., a measure that takes the value 1 for events that contain the sample  $x$  and zero otherwise. Under these assumptions, the expected value of any function of  $\zeta$  can be computed as:

$$\mathbb{E}\{f(\zeta)\} = \int_{\Delta} f(\zeta) d\mathcal{P} = \sum_{i=1}^n w_i \cdot f(\zeta_k). \quad (16)$$

where  $f(\cdot)$  is a well-behaved function. The accuracy in approximating the stochastic integral  $\mathbb{E}\{f(\zeta)\} = \int_{\Delta} f(\zeta) d\mathcal{P}$ , with  $\sum_{i=1}^n w_i \cdot f(\zeta_k)$ , largely depends on the technique employed to discretize uncertain parameters, i.e., selection of  $\zeta_i$  and  $w_i$ . The choice of a suitable discretization method is dependent on the specific characteristics of the problem and the required level of approximation accuracy. Monte Carlo (González-Arribas et al., 2018) and generalized polynomial chaos (Debusschere et al., 2004) are two of the most commonly used approaches in the literature.

Under the performed discretization, one can include the dynamical equations for generating the trajectories associated with the  $k$ th sample of uncertainty ( $\zeta_k$ ) and the corresponding initial conditions (denoted as  $\{\mathbf{x}_k(t), \mathbf{u}_k(t), \mathbf{z}_k(t)\}$ ) into a newly defined augmented dynamical model as:

$$\underbrace{\begin{bmatrix} \dot{\mathbf{x}}_1(t) \\ \dot{\mathbf{x}}_2(t) \\ \vdots \\ \dot{\mathbf{x}}_n(t) \end{bmatrix}}_{\mathbf{x}_a(t)} = \underbrace{\begin{bmatrix} \mathbf{f}(\mathbf{x}_1(t), \mathbf{u}_1(t), \mathbf{z}_1(t), \zeta_1, t) \\ \mathbf{f}(\mathbf{x}_2(t), \mathbf{u}_2(t), \mathbf{z}_2(t), \zeta_2, t) \\ \vdots \\ \mathbf{f}(\mathbf{x}_n(t), \mathbf{u}_n(t), \mathbf{z}_n(t), \zeta_n, t) \end{bmatrix}}_{\mathbf{f}_a(\mathbf{x}_a(t), \mathbf{u}_a(t), \mathbf{z}_a(t), t)} \quad (17)$$

where the augmented vectors of control and algebraic variables are defined as

$$\mathbf{u}_a(t) = [\mathbf{u}_1(t), \dots, \mathbf{u}_n(t)]^T, \quad \mathbf{z}_a(t) = [\mathbf{z}_1(t), \dots, \mathbf{z}_n(t)]^T. \quad (18)$$

Similarly, the path constraints in Eqs. (9), (10) are now enforced for each scenario (i.e., each realization of uncertainty within the sampled space):

$$\mathbf{h}_a(\mathbf{x}_a(t), \mathbf{u}_a(t), \mathbf{z}_a(t), \delta) = \begin{bmatrix} \mathbf{h}(\mathbf{x}_1(t), \mathbf{u}_1(t), \mathbf{z}_1(t), \zeta_1, t) \\ \mathbf{h}(\mathbf{x}_2(t), \mathbf{u}_2(t), \mathbf{z}_2(t), \zeta_2, t) \\ \vdots \\ \mathbf{h}(\mathbf{x}_n(t), \mathbf{u}_n(t), \mathbf{z}_n(t), \zeta_n, t) \end{bmatrix} \quad (19)$$

$$\mathbf{g}_a(\mathbf{x}_a(t), \mathbf{u}_a(t), \mathbf{z}_a(t), \delta) = \begin{bmatrix} \mathbf{g}(\mathbf{x}_1(t), \mathbf{u}_1(t), \mathbf{z}_1(t), \zeta_1, t) \\ \mathbf{g}(\mathbf{x}_2(t), \mathbf{u}_2(t), \mathbf{z}_2(t), \zeta_2, t) \\ \vdots \\ \mathbf{g}(\mathbf{x}_n(t), \mathbf{u}_n(t), \mathbf{z}_n(t), \zeta_n, t) \end{bmatrix} \quad (20)$$

and finally, using Eq. (16), the cost functional and boundary conditions can be written as

$$\min_{\mathbf{u}_a(t)} J_a = M_a(t_0, t_f, \mathbf{x}_a(t_0), \mathbf{x}_a(t_f)) + \int_{t_0}^{t_f} L_a(\mathbf{x}_a(t), \mathbf{u}_a(t), \mathbf{z}_a(t)) dt \quad (21)$$

$$M_a(t_0, t_f, \mathbf{x}_a(t_0), \mathbf{x}_a(t_f)) = \sum_{i=1}^n w_i \cdot M(t_0, t_f, \mathbf{x}_i(t_0), \mathbf{x}_i(t_f)) \quad (22)$$

$$L_a(\mathbf{x}_a(t), \mathbf{u}_a(t), \mathbf{z}_a(t), t) = \sum_{i=1}^n w_i \cdot L(\mathbf{x}_i(t), \mathbf{u}_i(t), \mathbf{z}_i(t), t)$$

$$\Psi_a(t_0, t_f, \mathbf{x}_a(t_0), \mathbf{x}_a(t_f)) = \sum_{i=1}^n w_i \cdot \Psi(t_0, t_f, \mathbf{x}_i(t_0), \mathbf{x}_i(t_f)). \quad (23)$$

As for tracking conditions, let us define  $\mathbf{x}_i(t)$ ,  $\mathbf{u}_i(t)$ ,  $\mathbf{z}_i(t)$  as vectors including tracked state, tracked control and tracked algebraic variables. Then, one can impose tracking conditions for different scenarios as

$$T_x \mathbf{x}_i(t) = \mathbf{x}_i(t) \quad (24)$$

$$T_u \mathbf{u}_i(t) = \mathbf{u}_i(t) \quad (25)$$

$$T_z \mathbf{z}_i(t) = \mathbf{z}_i(t) \quad (26)$$

for  $i = 1, \dots, n$ . Under these approximations and reformulations, the robust optimal control problem has been converted to a deterministic one with a larger dimension. From the implementation point of view, as will be shown in the next section, instead of duplicating both tracked and untracked variables and then imposing tracking conditions for tracked variables, it is computationally more efficient to duplicate only untracked variables when building the augmented dynamical model. In this respect, we will receive unique profiles for tracked variables without requiring additional path constraints and adding extra dimensions corresponding to tracked variables. It should be noted that a feasible solution may not always exist, and it highly depends on the dynamical model of the system and the way it is represented; having a unique trajectory for all possible realizations of uncertainties may not always be possible. In the next section, we will make some definitions and reformulations allowing us to efficiently utilize this approach for the robust climate-optimized flight planning problem.

All in all, the primary robust optimal control problem represented by Eqs. (7)–(14) has been converted into a deterministic optimization problem with the cost functional given in Eq. (21) to be minimized with the augmented control vector  $\mathbf{u}_a(t)$  subject to dynamical constraints (i.e., dynamical model of the system expanded by finite scenarios representing uncertainty), equality and inequality path constraints, and boundary conditions given in Eqs. (17), (19), (20), (23), respectively.

#### 4. Robust 4D climate-optimal aircraft trajectory planning

In this section, we model the climate-optimal flight planning problem under the framework presented in Section 3. The uncertainty in the forecasted wind and temperature perturbs the aircraft's dynamical behavior. In addition, the uncertainty in the meteorological variables required for calculating aCCFs is propagated when calculating objectives in the defined cost functional (see Sub Section 2.4). In the context of flight planning, it is required to determine a unique flight plan, i.e., a unique lateral route in latitude and longitude that starts and ends at predefined points in space, as well as having a fixed altitude profile and a fixed

airspeed schedule. Therefore, despite the existence of uncertainty, we need to optimize a deterministic flight plan. In our definition, the tracked variables are those variables that exclude uncertainty effects. Thus, lateral path, altitude, and speed are designated as tracked variables within the robust optimal control formulation presented in Section 3. In this respect, control policies are to be generated such that these states of the aircraft dynamical model follow a unique profile for all probable realizations of weather conditions represented employing ensemble weather forecasts. However, with the current formulation of the dynamical model, the tracking condition can only be satisfied if all ensemble members are identical. This is due to the fact that flight time is considered as an independent variable for the aircraft dynamical model given by Eq. (2), implying that it will be unique for all scenarios. The uniqueness of flight time in all scenarios means that the aircraft's position is fixed with respect to time, considering all possible realizations of wind, which is not realistic. Therefore, direct application of the methodology presented in Section 3 without modifying the aircraft dynamical model is not feasible.

To address the requirements in an operationally feasible manner, we start by defining the ground speed ( $v_{gs}$ ) and the course ( $\psi$ ) as additional (untracked) algebraic and (tracked) control variables, respectively, with the standard composition of velocities relating those two additional variables to airspeed, heading, and wind:

$$v_{gs} \cos(\psi) = v_{tas} \cos(\chi) + w_y, \quad v_{gs} \sin(\psi) = v_{tas} \sin(\chi) + w_x. \quad (27)$$

where  $v_{gs}$  is constrained to be greater than or equal to 0 to ensure the uniqueness of ground speed and course. To capture wind uncertainty in the flight time, we select the distance flown along the route as the independent variable and rewrite the dynamical model with respect to distance using  $\frac{dt}{ds} = v_{gs}^{-1}$  as

$$\frac{d}{ds} \begin{bmatrix} \phi \\ \lambda \\ h \\ v_{tas} \\ m \\ t \end{bmatrix} = \begin{bmatrix} \cos(\psi)(R_M(\phi) + h)^{-1} \\ \sin(\psi) \left( (R_N(\phi) + h) \cos(\phi) \right)^{-1} \\ v_{gs}^{-1} v_{tas} \sin(\gamma) \\ (T(C_T) - D(C_L))(v_{gs} \cdot m)^{-1} - v_{gs}^{-1} g \sin(\gamma) \\ -f_c(C_T)v_{gs}^{-1} \\ v_{gs}^{-1} \end{bmatrix}. \quad (28)$$

With this representation, by selecting time ( $t$ ) as an untracked variable, the effects of wind uncertainty can now be reflected in the flight time (through ground speed). We also define slopes of airspeed and altitude as tracked control variables ( $d_a$  and  $d_v$ , respectively). This is reasonable since, within the current dynamical model, the derivatives of tracked variables (i.e., altitude and true airspeed) are obtained from terms including both tracked and untracked variables. In this respect, after defining tracked control variables  $d_a$  and  $d_v$ , we need to transfer the dynamic relationships to two new equality constraints:

$$\begin{bmatrix} d_v \cdot v_{gs} \\ d_h \cdot v_{gs} \end{bmatrix} = \begin{bmatrix} (T - D)m^{-1} - g \sin(\gamma) \\ v_{tas} \sin(\gamma) \end{bmatrix}. \quad (29)$$

Considering the modifications made, the dynamical model can now be utilized by the methodology presented in Section 3.2. In the following, we formulate the robust climate-optimized flight planning problem by representing the aircraft dynamical model, path and boundary constraints, and objective function to include the effects of weather uncertainty characterized using an ensemble weather forecast.

#### 4.1. Augmented dynamical model

The solution approach presented in Section 3.2 is generic in the sense of the used weather forecast. For weather data characterized by uncertainty in a continuous distribution, a discretization step is required. In this study, however, we use an EPS weather forecast, directly representing uncertainty in a discrete distribution. Therefore, it is well-suited for the robust flight planning problem presented in Section 3 without requiring a discretization step. In this respect, the number of discretization samples corresponds to the number of ensemble members ( $N_{EPS}$ ), with each member being treated as a single sample ( $\zeta$ ). In addition, we assume that each member of an EPS carries equal probability ( $w_i = N_{EPS}^{-1}$  for  $i = 1, \dots, N_{EPS}$ ). This means that a weather pattern with a higher likelihood of occurrence is represented by more members in the ensemble.

Let us consider the vector of required meteorological variables with uncertainty as

$$\zeta := \mathbf{W}(\lambda, \phi, h, t(\delta), \delta) = [T \quad w_x \quad w_x \quad GH \quad F_{in} \quad PV \quad OLR \quad R]. \quad (30)$$

Employing EPS weather forecast with  $N_{EPS}$  ensemble members, we can represent the uncertainty with  $N_{EPS}$  samples, each associated to one ensemble member:

$$\zeta_i := \mathbf{W}_i(\lambda, \phi, h, t_i) := \mathbf{W}(\lambda, \phi, h, t(\delta_i), \delta_i) = [T_i \quad w_{x,i} \quad w_{x,i} \quad GH_i \quad F_{in,i} \quad PV_i \quad OLR_i \quad R_i] \quad (31)$$

where  $\mathbf{W}_i$  is a vector of meteorological variables corresponding to the  $i$ th ensemble member. In this respect, we can build an augmented aircraft dynamical model by including  $N_{EPS}$  copies (i.e., number of ensemble members) of the untracked state, control,

and algebraic variables, each corresponding to a possible realization of weather variables:

$$\frac{d}{ds} \begin{bmatrix} \phi \\ \lambda \\ h \\ v_{tas} \\ m_1 \\ \vdots \\ m_{N_{EPS}} \\ t_1 \\ \vdots \\ t_{N_{EPS}} \end{bmatrix} = \begin{bmatrix} \cos(\psi)(R_M(\phi) + h)^{-1} \\ \sin(\psi) \left( (R_N(\phi) + h) \cos(\phi) \right)^{-1} \\ d_h \\ d_v \\ -f_c(C_{T,1})v_{gs,1}^{-1} \\ \vdots \\ -f_c(C_{T,N_{EPS}})v_{gs,N_{EPS}}^{-1} \\ v_{gs,1}^{-1} \\ \vdots \\ v_{gs,N_{EPS}}^{-1} \end{bmatrix} \quad (32)$$

where the augmented state and control vectors are

$$\mathbf{x}_a = [\phi \quad \lambda \quad v \quad h \quad m_1 \quad \dots \quad m_{N_{EPS}} \quad t_1 \quad \dots \quad t_{N_{EPS}}]^T \quad (33)$$

$$\mathbf{u}_a = [d_v \quad d_h \quad \psi \quad \gamma_1 \quad \dots \quad \gamma_{N_{EPS}} \quad C_{T,1} \quad \dots \quad C_{T,N_{EPS}} \quad \chi_1 \quad \dots \quad \chi_{N_{EPS}}]^T.$$

As can be observed, lateral path, speed profile, and flight altitude are repeated once, while the time and aircraft mass are considered  $N_{EPS}$  times to reflect meteorological uncertainty. With such an approach to building the trajectory ensemble, we avoid imposing tracking conditions. The uniqueness of such variables of the flight plan is due to the consideration of scenario-dependent (untracked) control, state, and algebraic variables. Regarding the applicability of this methodology, we need to note that, in our practical context, the tracking of the optimized deterministic flight plan is enforced by the autopilot and Flight Management System in real-time rather than employing the determined scenario-dependent variables as the realization of the uncertainty is not known before committing to a specific plan.

#### 4.2. Path constraints

The conditions that are imposed over an optimization interval are path constraints. In the following, constraints representing the flight envelope and feasibility of the made modifications to make the aircraft dynamical model suitable for the methodology presented in Section 3 are given as follows:

$$\begin{bmatrix} v_{gs,1} \cos(\psi) \\ \vdots \\ v_{gs,N_{EPS}} \cos \psi \\ v_{gs,1} \sin(\psi) \\ \vdots \\ v_{gs,N_{EPS}} \sin(\psi) \\ \hline d_v \cdot v_{gs,1} \\ \vdots \\ d_v \cdot v_{gs,N_{EPS}} \\ \hline d_h \cdot v_{gs,1} \\ \vdots \\ d_h \cdot v_{gs,N_{EPS}} \end{bmatrix} - \begin{bmatrix} v_{tas} \cos(\chi_1) \cdot \cos(\gamma_1) + w_{y,1} \\ \vdots \\ v_{tas} \cos(\chi_{N_{EPS}}) \cdot \cos(\gamma_{N_{EPS}}) + w_{y,N_{EPS}} \\ v_{tas} \sin(\chi_1) \cdot \cos(\gamma_1) + w_{x,1} \\ \vdots \\ v_{tas} \sin(\chi_{N_{EPS}}) \cdot \cos(\gamma_{N_{EPS}}) + w_{x,N_{EPS}} \\ \hline T(C_{T,1}) - D(C_{L,1})m_1^{-1} - g \sin(\gamma_1) \\ \vdots \\ T(C_{T,N_{EPS}}) - D(C_{L,N_{EPS}})m_1^{-1} - g \sin(\gamma_{N_{EPS}}) \\ \hline v_{tas} \sin(\gamma_1) \\ \vdots \\ v_{tas} \sin(\gamma_{N_{EPS}}) \end{bmatrix} = \mathbf{0}, \quad \begin{bmatrix} v_{cas, \text{stall}} - v_{cas}(v_{tas}) \\ v_{cas}(v_{tas}) - v_{cas, \text{max}} \\ \hline C_{T, \text{min}} - C_{T,1} \\ \vdots \\ C_{T, \text{min}} - C_{T,N_{EPS}} \\ C_{T,1} - C_{T, \text{max}} \\ \vdots \\ C_{T,N_{EPS}} - C_{T, \text{max}} \\ \hline C_{L,1} - C_{L, \text{max}} \\ \vdots \\ C_{L,N_{EPS}} - C_{L, \text{max}} \\ \hline M(v_{tas}) - M_{\text{max}} \\ -v_{gs,1} \\ \vdots \\ -v_{gs,N_{EPS}} \\ \hline h - h_{\text{max}} \end{bmatrix} \leq \mathbf{0} \quad (34)$$

Regarding equality type constraints, relationships between wind, course, heading, airspeed, and ground speed (given in Eq. (27)) for different ensemble members and different realizations of untracked variables are imposed in the first block. The second and third

blocks represent dynamical relations for true airspeed and flight altitude (given in Eq. (29)), respectively, for different realizations of untracked variables. The limitations for calibrated airspeed, thrust and lift coefficients, Mach, and altitude (due to flight envelope given in Eq. (3)) are imposed as inequality path constraints. Notice that some of these constraints are repeated  $N_{\text{EPS}}$  to assure the satisfaction of the corresponding constraints for all probable realizations of untracked variables.

#### 4.3. Boundary constraints

Boundary constraints represent the initial and final states of aircraft. For our flight planning problem, we consider the following conditions

$$\left. \begin{aligned} [\phi \quad \lambda \quad v \quad h](0) &= [\phi_0 \quad \lambda_0 \quad v_0 \quad h_0], \\ [\phi \quad \lambda \quad v \quad h](s_f) &= [\phi_f \quad \lambda_f \quad v_f \quad h_f], \\ t_i(0) &= 0 \\ m_i(0) &= m_0 \\ m_{f,\min} &\leq m_i(s_f) \\ t_{f,\min} &\leq t_i(s_f) \leq t_{f,\max} \end{aligned} \right\} \forall i \in \{1, \dots, N_{\text{EPS}}\}. \quad (35)$$

which implies that the initial conditions for both tracked and untracked state variables are selected fixed. In contrast, only tracked variables are set to fixed values for the final conditions. The final flight time and final flight mass are considered free but to be optimized to satisfy predefined ranges. Although this study focuses on meteorological uncertainty, without loss of generality, departure time and initial aircraft mass can be considered with uncertainty, and it is straightforward to consider it within the current formulation.

#### 4.4. Objective function

We aim to determine an optimal aircraft trajectory under meteorological uncertainty and examine the trade-off between the operational cost and climate effects. To this end, considering equal weights for all possible realizations of uncertainty (i.e., ensemble members), by using Eq. (21), we can rewrite the cost functional Eq. (4) with respect to the augmented dynamical model of the aircraft as:

$$\begin{aligned} J &= \text{CI}_m \cdot \overline{\text{SOC}} + \text{CI}_{dp} \cdot \widetilde{\text{SOC}} + \text{EI}_m \cdot 10^{10} \cdot \overline{\text{ATR}} + \text{EI}_{dp} \cdot 10^{15} \cdot \widetilde{\text{ATR}} \\ \text{Expected SOC} : \quad \overline{\text{SOC}} &:= \frac{1}{N_{\text{EPS}}} \sum_{i=1}^{N_{\text{EPS}}} \text{SOC}_i \\ \text{Expected ATR} : \quad \overline{\text{ATR}} &:= \frac{1}{N_{\text{EPS}}} \sum_{i=1}^{N_{\text{EPS}}} \sum_{j=1}^4 \text{ATR}_{i,j} \\ \text{Dispersion SOC} : \quad \widetilde{\text{SOC}} &:= \frac{1}{N_{\text{EPS}}} \sum_{i=1}^{N_{\text{EPS}}} (\text{SOC}_i - \overline{\text{SOC}})^2 \\ \text{Dispersion ATR} : \quad \widetilde{\text{ATR}} &:= \frac{1}{N_{\text{EPS}}} \sum_{i=1}^{N_{\text{EPS}}} \left( \sum_{j=1}^4 \text{ATR}_{i,j} - \overline{\text{ATR}} \right)^2 \end{aligned} \quad (36)$$

for  $j \in \{\text{NO}_x, \text{H}_2\text{O}, \text{CO}_2, \text{Cont.}\}$ , where

$$\begin{aligned} \text{ATR}_{i,\text{NO}_x} &= \int_0^{s_f} \text{aCCF}_{i,\text{NO}_x}(s, \mathbf{x}_i(s)) \cdot \text{EI}_{i,\text{NO}_x}(s, \mathbf{x}_i(s)) \cdot \dot{m}_i(s) \cdot ds \\ \text{ATR}_{i,\text{H}_2\text{O}} &= \int_0^{s_f} \text{aCCF}_{i,\text{H}_2\text{O}}(s, \mathbf{x}_i(s)) \cdot \dot{m}_i(s) \cdot ds \\ \text{ATR}_{i,\text{CO}_2} &= \int_0^{s_f} \text{aCCF}_{i,\text{CO}_2} \cdot \dot{m}_i(s) \cdot ds \\ \text{ATR}_{i,\text{Cont.}} &= \int_0^{s_f} \text{aCCF}_{i,\text{Cont.}}(s, \mathbf{x}_i(s)) \cdot ds \end{aligned} \quad (37)$$

and

$$\text{SOC}_i := 0.75[t_i(s_f) - t_0] + 0.51[m_0 - m_i(s_f)] \quad (38)$$

where  $\mathbf{x}_i(\cdot)$  is a vector, including the atmospheric location of flights (i.e.,  $\lambda, \phi, h$ ), and flight time corresponding to  $i$ th ensemble member (i.e.,  $t_i$ ). Notice that the evaluation of the performance index is now based on the distance flown ( $s$ ) as the independent variable.

**Table 2**  
Size of resulting NLP problems.

Number of ...	Deterministic (Node = 40)	Robust (Node = 40)	Robust (Node = 80)
Equality constraints ( $n_g$ )	480	3315	6675
Inequality constraints ( $n_h$ )	364	3262	6502
NLP variables ( $n_\theta$ )	596	3431	6911
Number of non-zeros in ...			
Lagrangian Hessian	3617	25 847	52 207
Eq. constr. Jacobian	3523	26 023	52 663
Ineq. constr. Jacobian	1527	14 883	29 723

All in all, we can now state the deterministic optimal control problem formulated to represent the robust climate-optimized flight planning problem as:

$$\begin{array}{ll}
 \text{minimize} & \text{objective function } (J) \text{ Eq. (36)} \\
 \text{with respect to} & \left. \begin{array}{l} \text{dynamical constraints Eq. (32)} \\ \text{path constraints Eq. (34)} \\ \text{boundary conditions Eq. (35)} \end{array} \right\} \text{(DRFP)}
 \end{array}$$

which we solve by employing the direct trapezoidal optimal control method. The direct optimal control approach converts all aspects of a dynamical optimization problem into discrete forms, which, in the end, delivers a nonlinear programming problem (NLP) in the following general form (Betts, 2010):

$$\min_{\theta} J_{\text{NLP}}(\theta) \quad (39)$$

$$\text{s.t. } G_j(\theta) = 0 \quad j = 1, \dots, n_g \quad (40)$$

$$H_k(\theta) \leq 0 \quad k = 1, \dots, n_h \quad (41)$$

where  $\theta \in \mathbb{R}^{n_\theta}$  is the vector of decision variables in the NLP formulation. The functions  $G_j(\cdot)$  and  $H_k(\cdot)$  correspond to the equality and inequality constraints, respectively. The optimal solution to the formulated optimal control problem is now obtained through solving the resulting NLP problem. The conversion to the nonlinear programming problem provides the capability to solve highly nonlinear optimal control problems with nonlinear path and boundary constraints, which are daunting to deal with by utilizing other optimal control approaches, including dynamic programming and indirect optimal control (Simorgh et al., 2022b).

We note that the optimality of the NLP solutions can be affected by the number of ensemble members used to characterize uncertainty. This is due to the increase in dimensions, heightening the chance of converging to local optima. Direct optimal control methods often depend on the initial guess quality and the problem's conditioning (Betts, 2010). As we formulate the robust aircraft trajectory optimization problem, the state space dimension expands, increasing the NLP size (almost) linearly. To promote robust convergence, we propose an effective initial guess generation strategy, sequentially solving a series of problems with increasing complexity, where the solution of each problem initializes the subsequent one:

- Generate a 2D initial guess from the orthodromic path with the first forecast member (ensemble member 0).
- Solve the deterministic problem with constant altitude and constant airspeed with a low number of discretization nodes (initial resolution  $\mathcal{R}_0$ , defined as the number of collocation nodes used to convert the formulated optimal control problem to a nonlinear programming problem).
- Solve the deterministic problem with variable altitude and variable airspeed with higher resolution (intermediate resolution  $\mathcal{R}_1$ ).
- Solve the robust problem considering all ensemble members with variable altitude and variable airspeed at resolution  $\mathcal{R}_1$ .

In each step, the resulting solution is fed as an initial guess to the next step with suitable interpolations. The result of the last step is employed as the initial guess of the main problem. The main problem is similar to the last step in terms of settings but with a different resolution ( $\mathcal{R}_m$ ):  $\mathcal{R}_m \geq \mathcal{R}_1$ .

## 5. Simulation results

In this section, we explore the performance of our proposed robust trajectory optimization method for three different scenarios: scenario with (1) no formation of persistent contrails, (2) formation of cooling contrails, and (3) formation of warming contrails. We selected these three cases because of the strong variability, high uncertainty, and the dominant climate effects of contrails.

The aircraft is an A320-214 with an initial mass of 61600 kg. The direct optimal control method is employed here to solve the proposed robust flight planning problem. The trapezoidal rule is used for the transcription of dynamical optimization to an NLP problem, which is then solved by the IPOPT (Wächter and Biegler, 2006) solver in Python. For the trajectory optimizations performed in this study, we have selected the number of discretization nodes as  $\mathcal{R}_0 = 20$ ,  $\mathcal{R}_1 = 40$ , and  $\mathcal{R}_m = 80$ . The size of the

**Table 3**

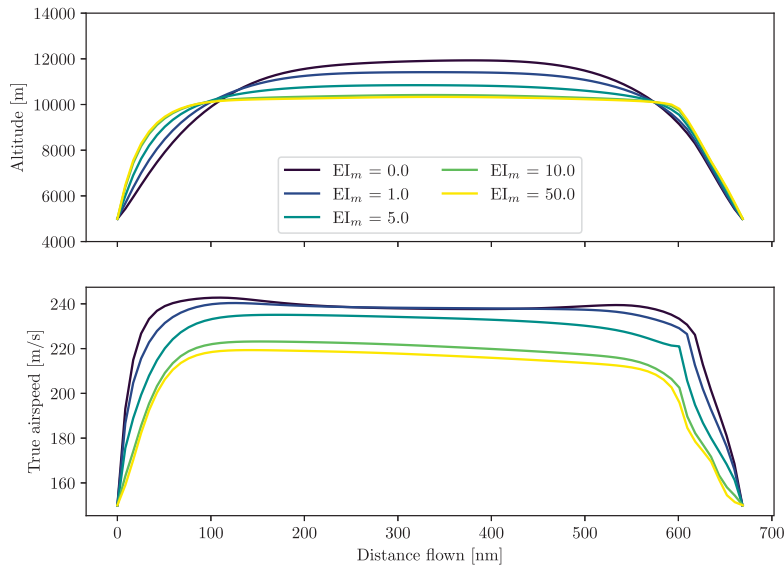
Performance of trajectories in terms of climate impact and operating cost for the three considered cases. Color code for uncertainty level: low (\*), medium (\*\*), high (\*\*\*). Color code for changes in the climate impact and operating cost compared to the cost-optimal routing option (i.e., EI=0): increase (↑), reduction (↓).

Scenario	EI <sub>m</sub>	EI <sub>d,p</sub>	Climate Effects					Operating Cost		
			ATR-H <sub>2</sub> O [1e-11 K]	ATR-CO <sub>2</sub> [1e-11 K]	ATR-NO <sub>x</sub> [1e-11 K]	ATR-Cont. [1e-11 K]	Net ATR (min – max) (Δ% v.s. EI = 0) [1e-11 K]	Time [min.]	Fuel Cons. [kg]	SOC (min, max) (Δ% v.s. EI = 0) [USD]
CASE 1	0.0	0.0	1.79	5.41	62.69	0	69.9 (69.8 – 69.95) (0%)	90.19	7747.61	8010.08 (80012 – 8019.5) (0%)
	1.0	0.0	1.73	5.38	58.14	0	65.27 (65.22 – 65.32) (–6.6%)	91.28	7703.98	8036.76 (8031.1 – 8046.78) (+0.33%)
	5.0	0.0	1.67	5.37	54.12	0	61.17 (61.14 – 61.22) (–12.5%)	94.41	7683.24	8167.01 (8163 – 8174.9) (+1.96%)
	10.0	0.0	1.66	5.369	51.80	0	58.82 (58.77 – 58.89) (–15.85%)	100	7676.81	8414.82 (8407.3 – 8426.4) (+5.05%)
	50.0	0.0	1.66	5.374	51.45	0	58.49 (58.44 – 58.56) (–16.32%)	101.78	7683.22	8498.94 (8490.6 – 8511.3) (+6.10%)
CASE 2	0.0	0.0	2.14	2.94	22.4	–10.32	17.16 (0.78 – 26.02) (0%)	111.12	4218.70	7152.00 (7140.27 – 7160.52) (0%)
	0.1	0.0	1.99	2.96	21.34	–23.37	2.933 (–14.60 – 12.37) (–82.9%)	112.18	4246.75	7214.03 (7204.60 – 7220.61) (+0.9%)
	10.0	0.0	1.11	3.29	18.89	–76.98	–53.7 (–70.7 – 34.52) (–412.7%)	113.37	4711.70	7504.87 (7494.59 – 7517.72) (+4.93%)
	50.0	0.0	1.01	3.32	18.13	–89.69	–67.2 (–91.1 – 45.49) (–491.5%)	117.40	4756.74	7709.17 (7700.27 – 7717.62) (+7.79%)
	70.0	0.0	1.16	3.64	19.51	–110.3	–86.0 (–105.5 – 62.98) (–601.1%)	130.24	5214.86	8520.77 (8512.56 – 8533.26) (+19.13%)
	50.0	1.0	1.12	3.39	20.25	–74.73	–49.96 (–57.92 – 41.26) (–391.0%)	121.40	4889.13	7956.74 (7942.90 – 7968.07) (+11.25%)
50.0	5.0	1.16	3.45	21.57	–60.71	–34.52 (–38.83 – 28.03) (–301.1%)	124.81	4969.93	8151.39 (8137.21 – 8163.18) (+13.97%)	
CASE 3	0.0	0.0	1.167	3.53	32.23	150.2	187.21 (165.6 – 242.8) (0%)	130.64	5066.29	8462.84 (8454.57 – 8472.75) (0%)
	1.0	0.0	1.166	3.54	32.22	114.5	151.4 (126.2 – 209.2) (–19.1%)	130.61	5077.07	8466.81 (8458.81 – 8476.35) (0.05%)
	10.0	0.0	1.158	3.54	32.32	70.20	107.23 (79.9 – 129.9) (–42.7%)	130.94	5081.77	8484.05 (8476.46 – 8492.86) (0.25%)
	30.0	0.0	1.162	3.61	31.44	26.72	62.93 (57.5 – 67.9) (–66.38%)	130.90	5176.27	8530.73 (8522.37 – 8537.89) (0.80%)
	50.0	0.0	1.189	3.69	31.57	0.68	37.14 (36.6 – 37.8) (–80.16%)	130.87	5291.96	8588.15 (8582.42 – 8595.21) (+1.48%)

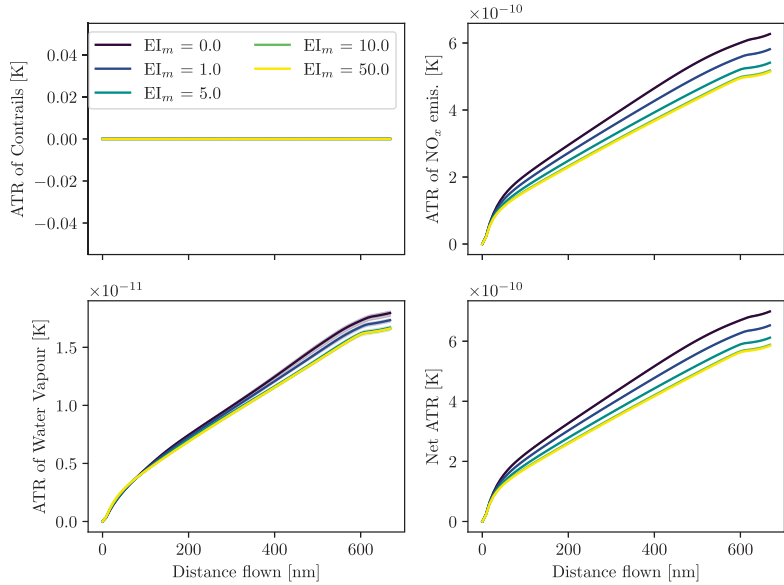
resulting NLP problems at each step is given in Table 2. It can be seen how the original robust problem is sequentially solved by feeding as initial guess, the resulting solution of relatively simpler problems.

For all three considered cases, the initial and final flight altitude and the initial and final true airspeeds are selected 5 km and 150 m/s, respectively, and the rest limiting constraints (e.g., maximum thrust coefficient and maximum Mach number) are provided using BADA4.2 specifications. The information on weather situation is obtained from the ERA5 data products<sup>3</sup> with ten ensemble members to characterize weather uncertainty. As for weighting parameters in the flight planning objective function, we consider the weights of the expected flight time and the expected fuel consumption as  $C_t = 0.75$  USD/s and  $C_f = 0.51$  USD/kg to represent the operating cost in a simplified manner in USD, called simple operating cost (Yamashita et al., 2020). We first focus on the average of objectives, i.e., assigning weighting parameters penalizing the variance of objectives (i.e.,  $CI_{d,p}$  and  $EI_{d,p}$ ) to 0. Then, the weight of average SOC (i.e.,  $CI_m$ ) is assigned to 1, and we perform optimization for different values of the parameter penalizing the average of climate effects (i.e.,  $EI_m$ ) to generate a Pareto-frontier. After analyzing the identified Pareto-optimal solutions, the decision to include the variance of climate effects and operating cost in the objective function is made. It should be noted that the selection of these weights is highly scenario-dependent, and one set of weighing parameters may not provide similar performance for different scenarios. Consequently, for each scenario, different sets of weighting parameters need to be considered for more efficient decision-making. Although in this study we directly assign different values for weights to generate Pareto-frontiers, the interested readers are referred to Lührs et al. (2021) and Simorgh et al. (2023) for different approaches to selecting these parameters. In these studies, all objectives are normalized with respect to appropriate reference values (generally their maximum values). Then, weights of objectives are selected such that the sum of all weights is equal to 1. With such an approach, the objectives can be efficiently prioritized.

<sup>3</sup> <https://cds.climate.copernicus.eu/>



(a) Flight altitude and true airspeed.



(b) ATRs associated with each non-CO<sub>2</sub> species and the net ATR (accumulated values along the route). Shaded areas illustrate uncertainty ranges due to uncertain meteorological conditions.

Fig. 2. Results of Case 1 (2018-06-27 00:00 UTC) for different  $EL_m$  values.

5.1. Case 1 : Marseille-Manchester flight on june 27, 2018 (0000UTC)

For the first case study, we optimize the trajectory of a flight from Marseille to Manchester on June 27, 2018, departing at 0000UTC. The detailed numerical results for this case study are given in (Table 3) (see Case 1). Due to the weather conditions, there is no probability of forming persistent contrails for this flight. We select  $CI_m = 1.0$ ,  $CI_{dp} = 0.0$ ,  $EI_{dp} = 0.0$  and change the parameter that penalizes the average climate impact, i.e.,  $EL_m$ . The flight altitude, true airspeed, and obtained climate effects for different weighting parameters are depicted in Fig. 2. It can be seen that the aircraft for the cost-optimal routing strategy flies at high altitudes, while as we penalize the expected climate impact, the flight altitude is reduced, and the aircraft flies with lower speeds. Fig. 2(b) shows that such behavior efficiently mitigates the climate effects of water vapor and NO<sub>x</sub> emissions and, consequently, net ATR. To explore that in more detail, let us show the lateral paths plotted with the aCCF of NO<sub>x</sub> emissions at different altitudes in Fig. 3. It can be seen that reducing the aCCF of NO<sub>x</sub> is possible by lowering flight altitudes. Therefore, the altitude of 10 km is the

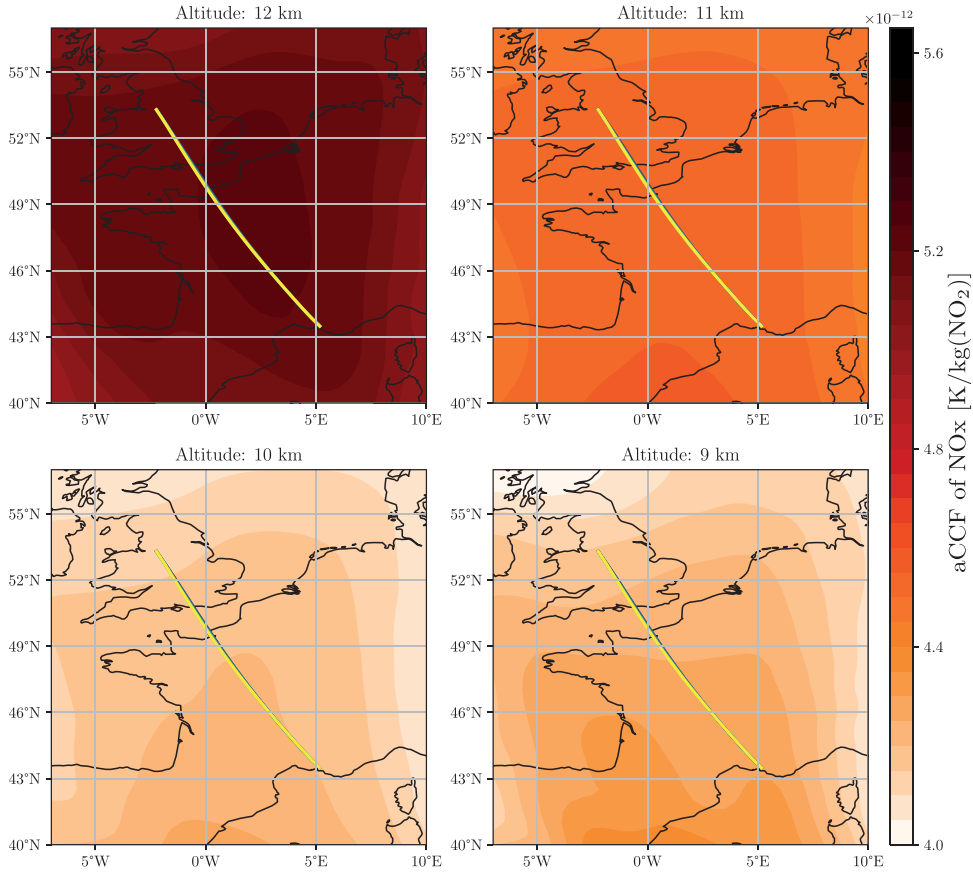


Fig. 3. Lateral paths with the mean of aCCF of NO<sub>x</sub> emissions as the colormap (Case 1).

best alternative which has been selected with  $EI_m = 50$ . In addition, the lateral paths are obtained almost similarly for all weighting parameters. Looking at the pattern of the aCCF of NO<sub>x</sub>, one can conclude that these functions behave smoothly at a given altitude. Therefore, the change of lateral path is not an efficient way of reducing the ATR from NO<sub>x</sub> emissions, taking into account the increased operating cost. To analyze the trade-off between operational cost and climate effects, trajectory optimization is performed for more weighting parameters and a Pareto-frontier is generated, shown in Fig. 4. It can be seen that for planning the aircraft trajectory with lower climate impact, we need to accept higher operating costs compared to the cost-optimal scenario. For this case, a 12.5% mitigation in climate effects can be obtained at the cost of a 2.96% increase in SOC. Another aspect of the results is the uncertainty in the climate effects and operating costs. Simorgh et al. (2023) reported that the variability among different members of the ERA5 data product, except for relative humidity, is low. The relative humidity is required to identify ice-supersaturated regions and, consequently, persisting contrails. Since no contrails are formed for this particular case, the uncertainty is almost negligible.

The results of optimizing this scenario can be summarized as follows:

- The aircraft flies at lower altitudes with lower speeds for the climate-optimal routing options compared to the cost-optimal one.
- The net climate effect is dominated by the impact of NO<sub>x</sub> emissions.
- The uncertainty in SOC and ATR is almost negligible.
- Changing the lateral path is not beneficial due to the smooth lateral behavior of NO<sub>x</sub> aCCF.

## 5.2. Case 2 : Frankfurt-Kyiv flight on december 20, 2018 (1200UTC)

For the next simulation, we consider a flight from Frankfurt to Kyiv on December 20, 2018, departing at 1200 UTC. The numerical results for this case study are provided in (Table 3) (see Case 2). Persistent contrails during the daytime reflect incoming solar radiation and may lead to a net cooling impact. For the considered scenario, there is a potential to form cooling contrails (based on the meteorological variable outgoing longwave radiation) using the aCCF of daytime contrails. Similar to the previous case, we start by selecting  $CI_m = 1.0$ ,  $CI_{dp} = 0.0$ ,  $EI_{dp} = 0.0$ , and change the parameter that penalizes the average climate impact. The vertical profile depicted in Fig. 5(a) shows that the aircraft flies at lower altitudes as we increase the penalty on climate effects. However,

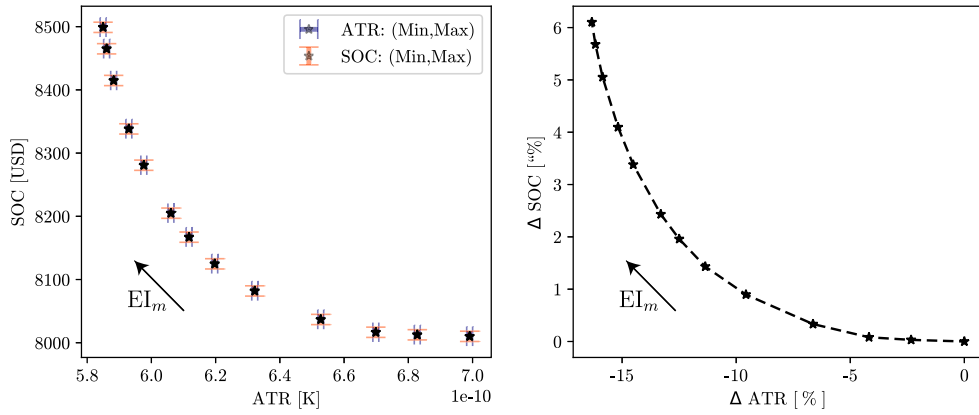


Fig. 4. Pareto-frontiers generated using different  $EI_m$  values (Case 1).

the speed profile has not changed considerably. Fig. 5(b) shows that the climate impact is reduced for this case study mainly by generating cooling contrails. The formation of cooling contrails is associated with significant uncertainty (see (Table 3), Case 2). As mentioned earlier, the variability of relative humidity within an EPS required to predict areas favorable to form persistent contrails is high, leading to considerable uncertainty in identifying PCFAs. This, in turn, increases the uncertainty in quantifying contrails climate impact. From Fig. 6, we conclude that the aircraft tends to fly through PCFAs to generate cooling contrails for large  $EI_m$ 's, thus associated with high uncertainty (see Fig. 5).

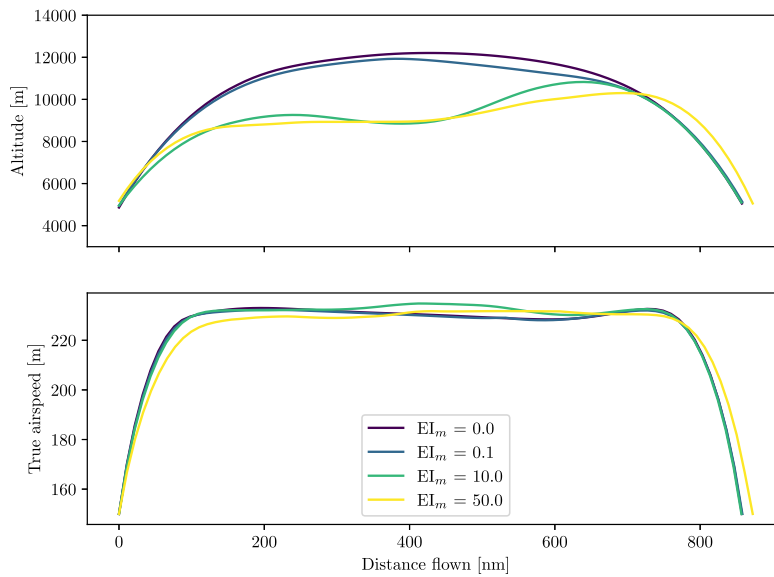
The Pareto-frontier in Fig. 7 shows the trade-off between SOC and ATR. It can be seen that due to the formation of cooling contrails, the climate-optimized routing strategy is beneficial by taking into account the relative increase in SOC (e.g., 82% reduction in climate impact with less than 1% increase in the operating cost for  $EI_m = 1$ ). However, the quantified ATRs are highly uncertain. To this end, we select  $EI_m = 50.0$  and add a penalty to the dispersion of ATR with two different values, i.e.,  $EI_{dp} = 1$  and 5. It can be seen in Fig. 8(b) that by including  $EI_{dp}$ , the dispersion of ATR decreases at the expense of reducing the average mitigation potential. To increase the predictability of ATR, the aircraft flew at an altitude with the maximum formation of cooling contrails (similar to  $EI_m = 50.0$ ,  $EI_{dp} = 0.0$ ) (see Fig. 8(a)) and changed the lateral path to avoid areas of airspace with high uncertainty in contrails ATR, characterized by the standard deviation of contrails aCCF (see Fig. 9). Fig. 7 shows the trade-off between these three routing options in terms of average cost, dispersion of cost, average ATR, and dispersion of ATR. It can be concluded that, for this particular case study, the increase in the predictability of climate effects comes at a higher expected operating cost and ATR (see (Table 3), Case 2, where  $EI_{dp} \neq 0$ ).

The results of optimizing this scenario can be summarized as follows:

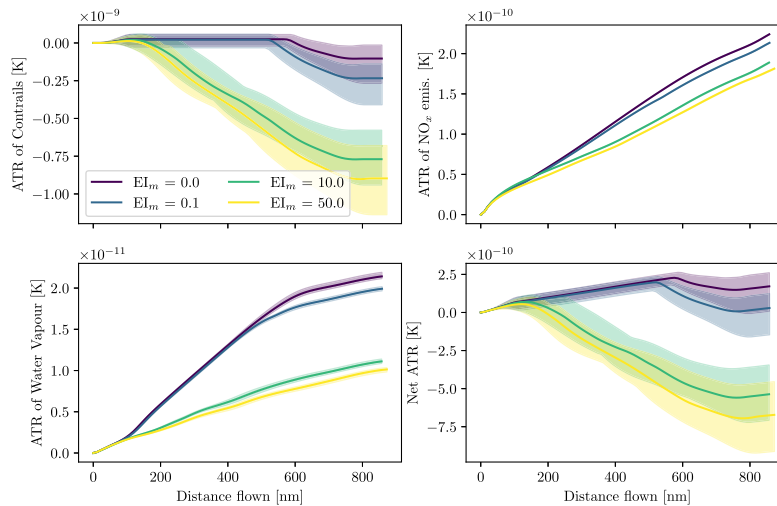
- The aircraft flies at lower altitudes for the climate-optimal routing option compared to the cost-optimal one.
- The aircraft changes its lateral path toward maximizing the generation of cooling contrails.
- The net climate impact is dominated by the impact of contrails.
- The uncertainty in SOC is negligible, and ATR is associated with high uncertainty due to the tendency to fly in PCFAs.
- By penalizing the variance of ATR in the objective function, there is a potential to obtain a less uncertain estimation of climate effects. However, one needs to consider the existing trade-off between predictability and average performance for cooling contrails.

### 5.3. Case 3 : Venice-Lisbon flight on june 18, 2018 (1200UTC)

A scenario in which warming contrails are formed with the cost-optimal routing option for a flight from Venice to Lisbon on June 18, 2018, departing at 1200 UTC, is analyzed. Table (3) (see Case 3) provides numerical results for this case study. Flight altitude, true airspeed, and the climate effects associated with each species for different values of the environmental index penalizing expected ATR are depicted in Fig. 10. Similar to previous cases, the aircraft flies at relatively lower altitudes for climate-optimal routing options (see Fig. 10(a)). From Fig. 10(b), we can see that contrails have dominant climate effects, and not only the mean value of net ATR but also the dispersion reduces as we penalize the expected ATR with larger weights. The reduction of ATR's dispersion with penalizing average values is not consistent with the previous scenario. This is due to the fact that, here, to reduce the climate impact of contrails (which has the largest effects), the aircraft tries to avoid producing warming contrails as the formation of cooling contrails is not possible. In this respect, the aircraft avoids flying in uncertain PCFAs. Thus, the uncertainty also reduces by penalizing average climate effects without requiring us to include the variance of ATR in the objective function. The mitigation potential is mainly obtained by re-routing warming contrails. This is because contrails have dominant climate effects and have non-smooth spatial patterns related to the inequality conditions to identify PCFAs. Thus, it is beneficial for trajectory optimization as large climate effects can be reduced by making efficient modifications to the vertical profile or/and lateral path. However, the



(a) Flight altitude and true airspeed.

(b) ATRs associated with each non-CO<sub>2</sub> species and the net ATR (accumulated values along the route). Shaded areas illustrate uncertainty ranges due to uncertain meteorological conditions.Fig. 5. Results of Case 2 (2018-12-20 12:00 UTC) for different  $EI_m$  values.

other species have more smooth patterns (see patterns of aCCFs illustrated in Fig. 17). Such a non-smooth pattern of contrails aCCF can be observed in Fig. 11, together with the determined lateral paths for different weights. It can be seen that all trajectories have selected almost similar lateral paths. By relating the flown altitudes (given in Fig. 10(a)) with the lateral paths, we conclude that at the beginning of the flight, in addition to the similar lateral routes, aircraft fly with similar altitude profiles as no contrails are formed. However, as soon as contrails start to form (see contrails climate effects given in Fig. 10(b)), trajectories associated with  $EI_m = 30$  and  $50$  reduce their altitudes to prevent forming warming contrails, leading to a large mitigation potential, in which, by accepting a 1.5% increase in operating cost, an 80% reduction in climate impact can be achieved (Fig. 12, Case 3 in Table (3), where  $EI_m = 50.0$ ). Therefore, changing altitude is more efficient than changing the lateral path for this scenario. This is because in order to fly at the altitudes selected by the cost-optimal routing option (i.e., 11–12 km), to avoid forming warming contrails, significant deviations from the shortest path will be required. In this case, despite large detours and, as a result, a considerable increase in the operating cost, the formation of warming contrails cannot be completely avoided. However, by sticking to the shortest path but flying at a lower altitude (9 km), no persistent contrails are generated (thus, no need for re-routing). Due to the complete avoidance of forming persistent contrails, the results (corresponding to  $EI_m = 30$  and  $50$ ) are almost deterministic.

The results of optimizing this scenario can be summarized as follows:

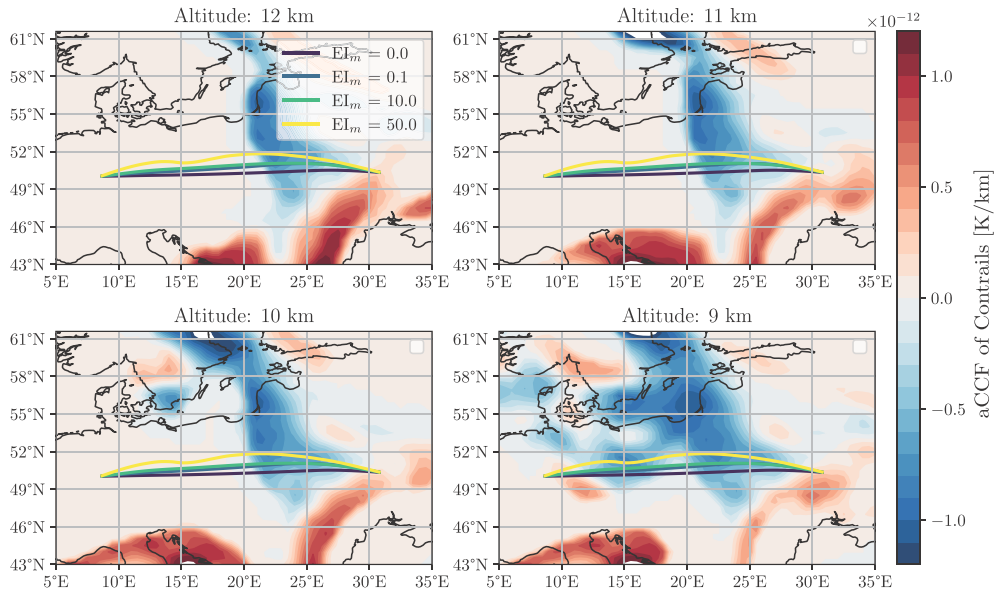


Fig. 6. Lateral paths with the mean of contrails aCCF as the colormap (Case 2).

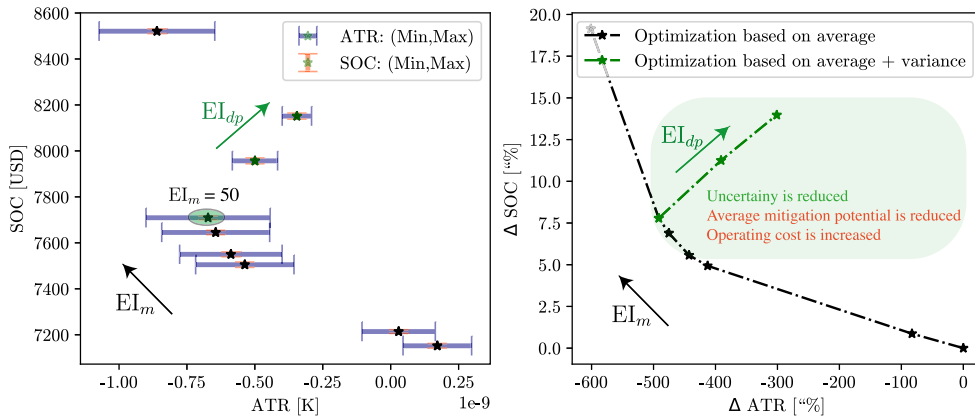


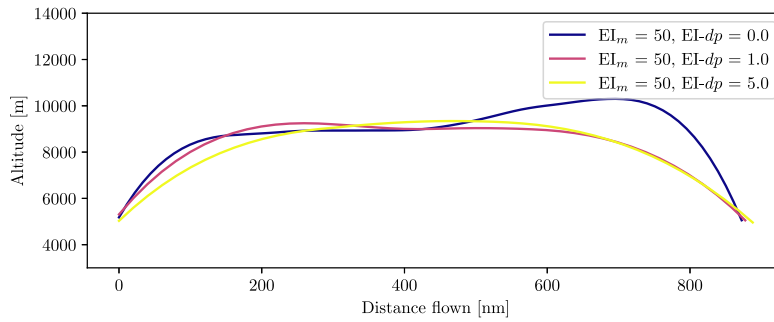
Fig. 7. Pareto-frontiers generated using different  $EI_m$  and  $EI_{dp}$  values (Case 2).

- The optimizer finds lower altitudes as a better alternative for the climate-optimal routing option compared to the cost-optimal one.
- The net climate effect is dominated by the impact of contrails.
- The climate effects of contrails are associated with high uncertainty.
- The reduction in climate impact is achieved mainly by re-routing warming contrails (by changing only the vertical profile).
- For the case that warming contrails can be generated, no trade-off exists between predictability and average performance; the uncertainty is also reduced by penalizing the average value of the net climate impact.

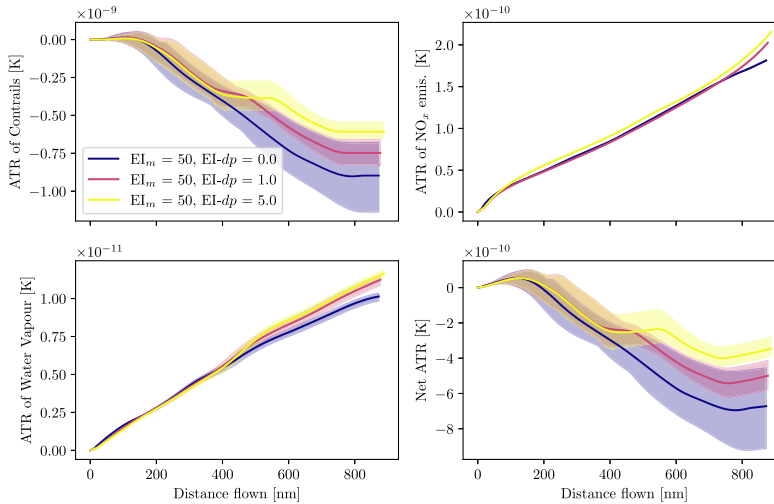
5.4. Discussion

In this paper, we explored the possibility of reducing climate effects with minimal sensitivity to meteorological uncertainty by efficient aircraft trajectory planning. In the following, we further discuss the obtained results, limitations of the optimizer, and the model used for climate impact estimations, as well as future lines of research.

- The scope of this study was to introduce a framework that can integrate meteorological uncertainty in planning climate-optimal trajectories. We conducted three case studies to demonstrate the performance of the proposed methodology. It is important to highlight that the achieved climate impact mitigations are specific to these particular cases and are not representative of other scenarios (e.g., different meteorological conditions and aircraft types). To comprehensively evaluate the potential for reducing



(a) Flight altitude.

(b) ATRs associated with each non-CO<sub>2</sub> species and the net ATR (accumulated values along the route). Shaded areas illustrate uncertainty ranges due to uncertain meteorological conditions.**Fig. 8.** Results of Case 2 (2018-12-20 12:00 UTC) for  $EI_m = 50$  and different  $EI_{dp}$ 's.

aviation-induced climate effects through flight planning, it is required to optimize realistic aerial traffic over a wide range of scenarios encompassing various aircraft types, geographic regions, and weather conditions. Furthermore, it is crucial to study the climate impact mitigation potential from a holistic network-level perspective rather than focusing solely on individual flights, as pointed out by Baneshi et al. (2023). When aircraft trajectories are optimized independently from each other, traffic patterns can significantly change toward avoiding climate-sensitive areas. This, in turn, may affect ATM performance, particularly in terms of sector demand, leading to increased ATC workload and complexity. Therefore, once climate-optimized routes are planned, it is imperative to evaluate them from the ATM perspective. If necessary, appropriate resolution strategies should be implemented to ensure the stability of aerial traffic while striving to maintain climate optimality as closely as possible to the individually optimized flight trajectories. With such analysis, the climate impact mitigation potential can be evaluated in a more realistic manner. In our future research, we aim to address the problem of climate-friendly flight planning from the ATM perspective for large-scale scenarios.

- We note that the three case studies, while not encompassing all possible real-world scenarios, serve as representative examples of how the trajectory optimizer behaves in response to various situations, i.e., no formation of persistent contrails with the cost-optimal routing option, formation of warming contrails, and lastly, the possibility to generate cooling contrails. To illustrate that, we optimized the top 50 routes in 2018 (ranked using available seat kilometers (ASK) (Mendiguchia Meuser et al., 2022)) depicted in (Fig. 13) on two different days and departure times: December 20, 2018 (1200UTC) and June 18, 2018 (0000UTC). The numerical results for both cases are given in (Table 4) for different weighting parameters. Since the achieved mitigations are related mainly to contrails, we show the locations where persistent contrails (cooling/warming) are formed in Figs. (14, 15) for December 20, 2018 (1200UTC) and June 18, 2018 (0000UTC), respectively. It can be seen that, for the night-time flights (i.e., June 18, 2018 (0000UTC)), the formation of warming contrails is reduced with the climate-optimal routing options. However, for the daytime scenario, by increasing the weight penalizing average climate impact, in addition to avoiding forming warming contrails, cooling contrails are generated. Regarding uncertainty effects, similar to other case studies considered in

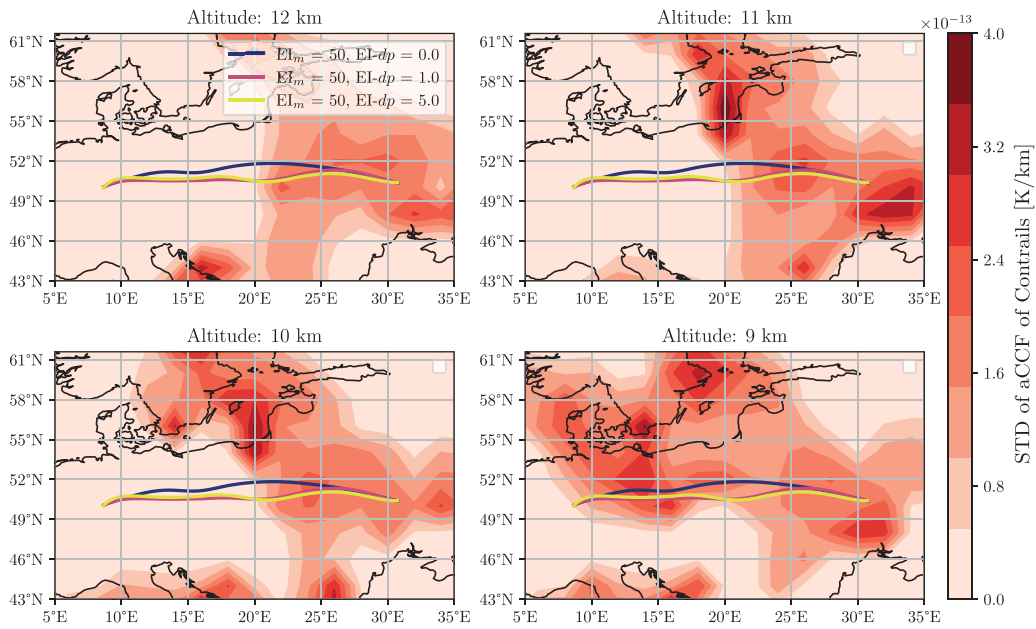


Fig. 9. Lateral paths with the standard deviation of contrails aCCF as the colormap (Case 2).

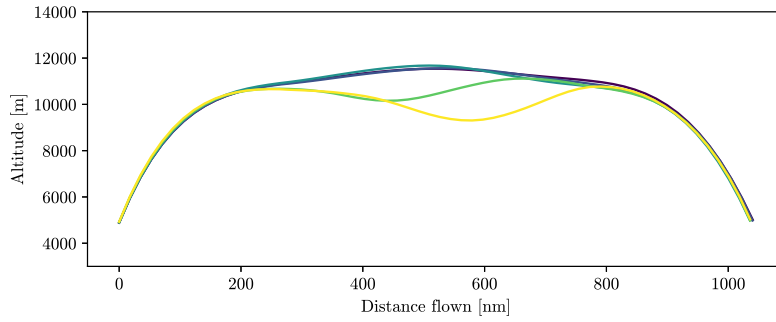
Table 4

Performance of the optimized top 50 routes in terms of climate impact, operating cost and flown altitudes for two different scenarios. Notice that the results are reported per flight. Color code for uncertainty level: low (\*), medium (\*), high (\*). Color code for changes in the climate impact and operating cost compared to the cost-optimal routing option (i.e., EI = 0): increase (\*), reduction (\*).

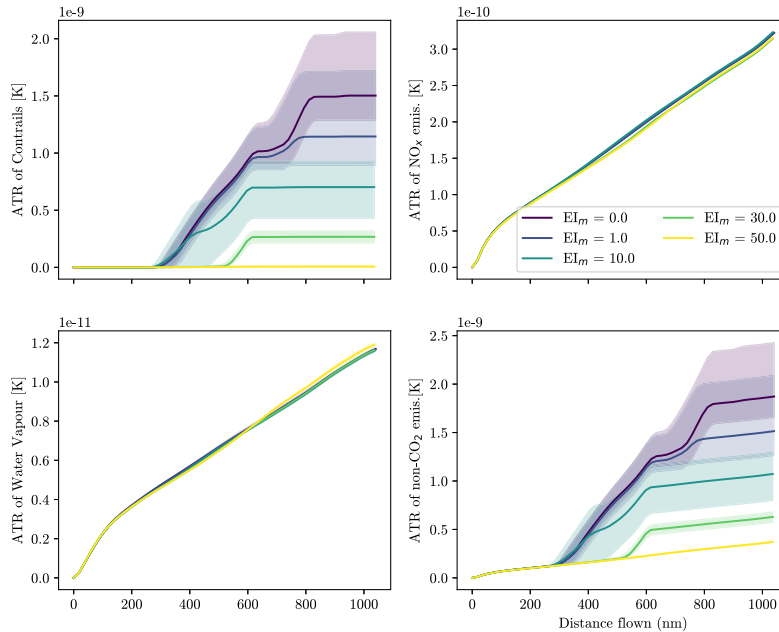
Scenario	EI <sub>m</sub>	Climate Effects					SOC (min, max) (Δ% v.s. EI = 0)[USD]	Flight Altitude [m]
		ATR-H <sub>2</sub> O [1e-11 K]	ATR-CO <sub>2</sub> [1e-11 K]	ATR-NO <sub>x</sub> [1e-11 K]	ATR-Cont. [1e-11 K]	Net ATR (min - max) (Δ% v.s. EI = 0) [1e-11 K]		
20-12-2018 (1200UTC)	0.0	2.37	3.55	25.1	9.75	40.78 (38.42 – 43.94) (0%)	8518.57 (8517.42 – 8520.36) (0%)	11 133.12
	1.0	2.35	3.55	24.9	1.82	32.68 (30.57 – 34.99) (–20.03%)	8527.09– (8525.1 – 8530.72) (+0.099%)	11 067.03
	10.0	2.10	3.63	23.66	–5.9	23.46 (21.2 – 26.64) (–42.58%)	8603.74 (8601.2 – 8604.87) (+0.98%)	10 613.30
	50.0	1.87	3.73	22.83	–9.82	18.62 (14.21 – 23.16) (–54.43%)	8722.55 (8721.08 – 8723.01) (+2.39%)	10 141.38
18-06-2018 (0000UTC)	0.0	2.0	3.53	28.7	45.01	79.33 (73.20 – 87.79) (0%)	8398.66 (8398.01 – 8399.82) (0%)	11 139.71
	0.1	2.0	3.53	28.75	34.05	68.3 (61.38 – 74.67) (–13.84%)	8402.86 (8401.32 – 8404.01) (+0.049%)	11 083.93
	10.0	1.98	3.56	28.60	19.03	53.19 (47.54 – 59.14) (–32.95%)	8423.85 (8423.02 – 8424.52) (+0.29%)	10 869.91
	50.0	1.75	3.61	27.9	8.84	42.11 (39.76 – 45.88) (–46.91%)	8499.74 (8498.23 – 8500.12) (+1.20%)	10 468.82

this work, avoiding warming contrails reduced the uncertainty effects while generating cooling contrails resulted in lower confidence in the climate impact estimates (see Pareto-frontier given in Fig. (16)). All in all, similar conclusions to individual cases can be drawn for the optimization of the top 50 routes.

- The optimization method proposed in this study offers a remedy for flight dispatchers aiming to plan climate-optimized trajectories with an increased level of reliability when there is significant uncertainty in the weather forecast. This approach enables utilizing weather forecasts that include uncertainty quantification (e.g., an ensemble prediction system) in the flight planning problem to generate uncertainty-aware climate-optimized trajectories (see, e.g., Fig. (7) of the paper). Therefore, the proposed methodology involves the pre-tactical flight planning phase (by pre-tactical, in this context, we refer to three hours before departure).



(a) Flight altitude and true airspeed.

(b) ATRs associated with each non-CO<sub>2</sub> species and the net ATR (accumulated values along the route). Shaded areas illustrate uncertainty ranges due to uncertain meteorological conditions.**Fig. 10.** Results of Case 3 (2018-06-18 12:00 UTC) for different  $EI_m$  values.

- To solve the proposed robust aircraft trajectory optimization problem, we include meteorological uncertainty in the dynamical model of the aircraft, leading to an increase in dimensions. This, in turn, degrades the computational performance compared to a deterministic trajectory optimization problem; therefore, in order to make this methodology applicable for large-scale scenarios (e.g., optimizing 30,000 daily flights), computational enhancements (e.g., parallelization on GPU) are required.
- We used the ensemble weather forecast to characterize uncertainty in the meteorological variables, directly representing uncertainty in a discrete distribution. Therefore, no discretization is performed. In the case of inputting weather data characterized by uncertainty in a continuous distribution, the accuracy of the solutions is affected by the choice of discretization method (e.g., Monte Carlo, Generalized polynomial chaos, etc.) and the number of discretization samples. An ideal approach would be one capable of accurately approximating the (continuous) distribution with a low number of samples. This is because the size of the optimization problem grows (almost) proportionally with the number of samples.
- Our results lead to the natural emergence of additional research questions. For the proposed method to progress further toward practical operations, additional empirical work must assess the relationship between EPS-modeled uncertainty and actually realized deviations from the forecasted field. This is because the studied technique exploits the structure of the uncertainty modeled by the EPS, thus sensitive to its accuracy.
- The findings of this study indicate potential trade-offs between operating costs and climate effects, as well as between expected performance and predictability. Understanding these trade-offs is essential for making informed decisions. For instance,

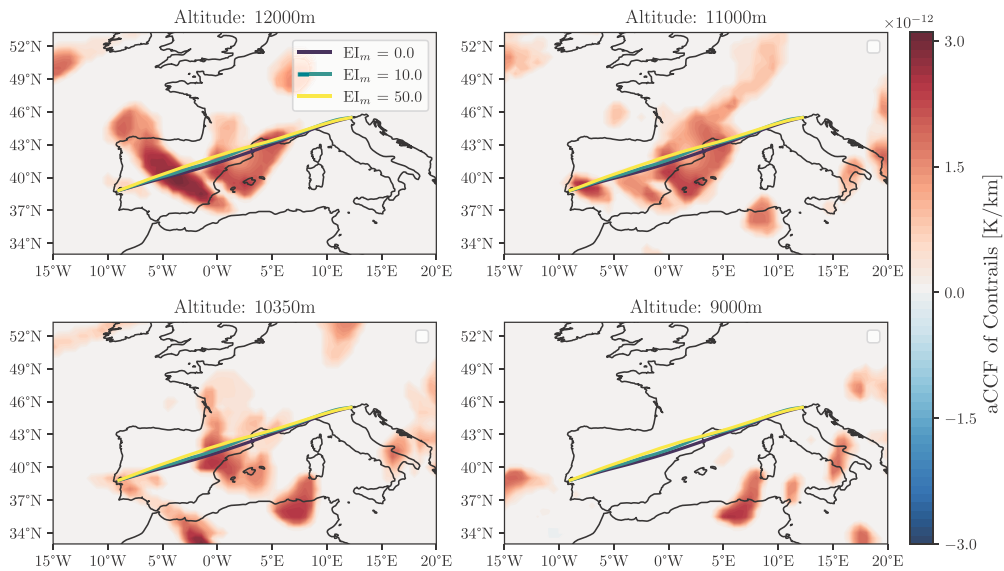


Fig. 11. Lateral paths with the mean of contrails aCCF as the colormap (Case 3).

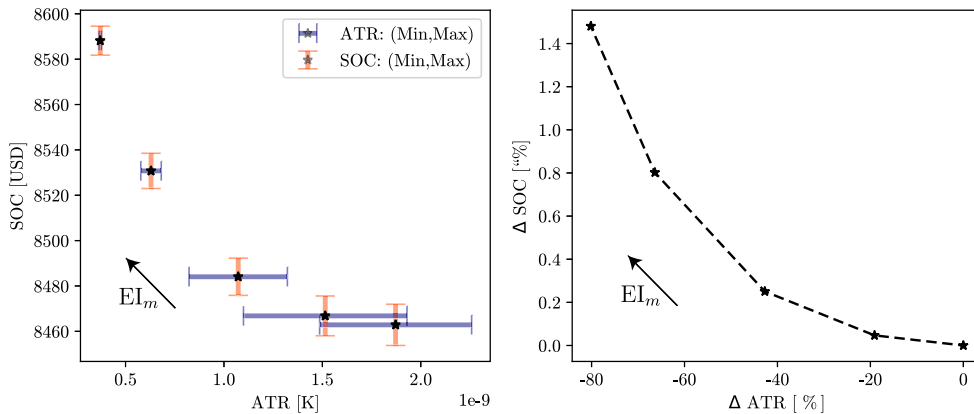


Fig. 12. Pareto-frontiers generated using different  $EI_m$  values (Case 3).

nowadays, the consideration of monetary costs (e.g., taxes and charges) for non- $CO_2$  climate effects is under exploration (within the market-based instruments, such as emissions trading schemes (ETS) or Carbon Offsetting and Reduction Scheme for International Aviation (CORSIA)) in order to relax the first trade-off (between climate effects and cost), leading to the possibility of identifying win-win situations (i.e., reducing both cost and climate impact compared to business-as-usual routing option) (Niklaß et al., 2021). As for predictability and the expected performance of climate effects, as a first step, other sources of uncertainties (e.g., different ways of estimating climate effects and emission calculation) need to be identified and included in flight planning in order to draw reliable conclusions. In the case of meteorological uncertainty, it was shown that a trade-off exists between expected performance and uncertainty for the scenario with the formation of cooling contrails. However, in the case of forming warming contrails, reducing the expected performance led to squeezing uncertainty ranges. Studying such alternative solutions helps to make more efficient decisions or set up policies. For example, an airline might prioritize choosing a flight path that offers significant potential for mitigating climate impact, even though a high level of uncertainty is involved. This choice may be preferred over a trajectory with a higher confidence level, which would come at the expense of increased operating costs and reduced average potential for climate impact mitigation (see, e.g., Fig. 7).

- Regarding the model used to estimate climate effects, it is important to highlight that the aCCFs were initially developed for summer and winter weather patterns, specifically focusing on the North Atlantic flight corridor. Consequently, employing the aCCFs for other seasons and regions necessitates careful consideration. Nonetheless, ongoing research is actively advancing the refinement of the aCCFs, including broadening their geographical coverage and accounting for a broader range of weather patterns.

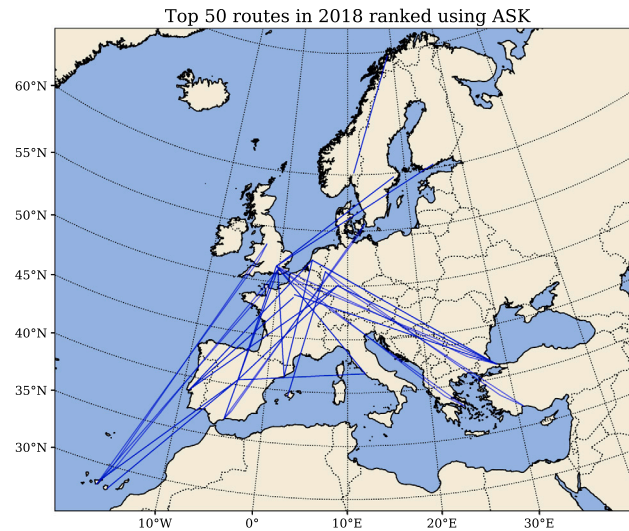


Fig. 13. Distribution of the top 50 routes in 2018 using ASK considered for trajectory optimization.

- For the considered case studies, it was shown that the methodology is capable of resulting in climate impact mitigations with reduced sensitivity to probable deviations in meteorological conditions. However, it is important to highlight that the reliability of the achieved climate benefits is highly dependent on several factors, including the reliability of climate impact estimates, the quality of the ensemble weather forecast, the accuracy of the engine emissions calculation (e.g.,  $\text{NO}_x$  emissions), and flyability of the optimized flight plan. In this respect, steps toward verification of these components are needed, which is a complex multi-disciplinary task. Regarding climate impact estimates, it is not possible to directly measure the climate effects. Only visible contrails can be detected using satellite and ground-based cameras. Indeed, verification of the climate impact of contrails is planned in several ongoing projects or in-situ measurements of ISSR (e.g., IAGOS dataset). As for aCCFs, they are continuously updated to improve the climate impact estimates. The latest version of aCCFs (i.e., V1.0a) was compared and calibrated toward the state-of-the-art climate-response model that considers averaged annual near-surface temperature change (Matthes et al., 2023). Regarding the feasibility of the planned climate-optimized trajectory, one of the contributions of this study is the development of a trajectory optimization technique supporting planning routes within the context of a future fully free-routing context. Therefore, it cannot be directly applied to the current structured airspace. All in all, it is necessary to verify the outcomes of research and transition them toward more operational endeavors (i.e., increasing TRL (Technology Readiness Level)).
- For contrail persistence, the ambient air needs to be supersaturated with respect to ice (relative humidity over ice  $> 100\%$ ). Strong variability in the relative humidity field is evident in ensemble simulations (see, e.g., Fig. 1 or (Simorgh et al., 2023; Simorgh and Soler, 2022)), indicating that this meteorological variable is forecasted with less confidence compared to such as temperature and geopotential (that are also relevant for calculating climate effects). Several studies reported an underprediction of the degree of ice supersaturation in numerical weather models (using, e.g., ERA-5 reanalysis data) due to the problematic forecast of relative humidity fields in the upper troposphere and lower stratosphere (UTLS) (e.g., see Gierens et al. (2020)). In particular numerical weather prediction models are weakly supersaturated ( $\text{RHi} \approx 100\%$ ) and underestimate regions with very high supersaturations ( $\text{RHi} > 120\%$ ) (Gierens et al., 2020; Schumann et al., 2021; Reutter et al., 2020). Having such a level of uncertainty and bias in identifying ice-supersaturated regions underlines the importance of additional in-situ measurements in the UTLS region for accurate assimilation of ice supersaturation and also an improvement of numerical weather model processes.
- In this study, we used aCCFs for climate-optimized flight planning. Contrail aCCFs were developed based on radiative forcing calculations on Lagrangian trajectories using ERA5 data (see the supplementary materials of Yin et al. (2023)). As mentioned in the introduction, “gridded” CoCiP ((Shapiro et al., 2022): domain-filling version of the Lagrangian CoCiP version (Schumann, 2012)) is an alternative that can be used for mitigating the climate effect of contrail-cirrus. In the following, we briefly discuss some differences between gridded CoCiP and contrail aCCFs. To estimate the climate effect using contrail aCCFs, meteorological input data only at the time of emissions are required. This makes technical implementation very easy. However, in the case of using gridded CoCiP (which is integrated into the Python package pycontrails), meteorological input data from several time steps are needed (covering the user-specified maximum age of contrails). Thus this requires a different data architecture and increases the computational effort. Moreover, the assumptions on contrail properties, lifetime, etc., differ for both approaches, leading to different estimates of contrail RF. An advantage of the aCCFs concept is the possibility to estimate the climate effects of other relevant non- $\text{CO}_2$  species, including  $\text{NO}_x$ -induced methane and ozone and water vapor emissions, while gridded CoCiP only quantifies the contrails effect. In addition, the aCCFs estimate climate effects using the state-of-the-art physical climate

### Optimization of Top 50 routes on June 18, 2018 (0000UTC)

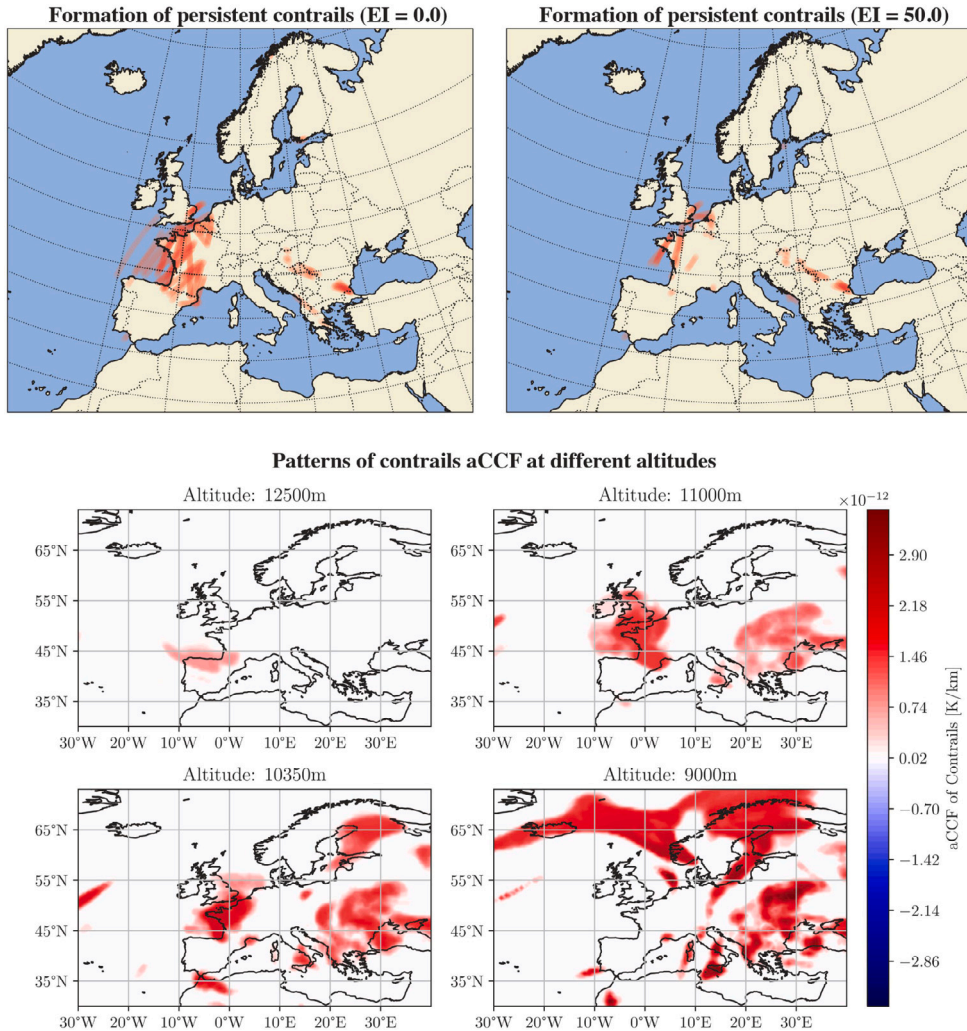


Fig. 14. Formation of persistent contrails (cooling (●)/warming (●)) along the flight path for the optimized top 50 routes on June 18, 2018 (0000UTC).

metric ATR. In contrast, CoCiP estimates the climate effect of contrails using the metric energy forcing (Schumann et al., 2011), defined as the integration of radiative forcing (multiplied by the length and width of contrails) over the lifetime. These two different metrics can simply be converted to each other. Unlike aCCFs, which were designed over the North Atlantic flight corridor in winter and summer months, gridded CoCiP development is valid globally without restrictions to seasons. A more comprehensive comparison between CoCiP and aCCF (of contrails) and a quantitative estimate of disparities in estimating the climate impact of contrails is an ongoing research (e.g., within CICONIA<sup>4</sup> project).

- The trajectory optimization approach presented in this study is designed for an idealized fully free-routing airspace where unconstrained determination of both lateral path and altitude is possible. In this respect, the optimizer seeks aircraft trajectories, minimizing the selected objective function. However, such an approach can sometimes lead to flight profiles that may not align seamlessly with the practicalities of current air traffic management operations. For example, frequent aircraft maneuvering during the cruise phase is generally discouraged in real-world operations, as it could negatively impact passenger comfort. Moreover, while the concept of free route airspace does permit more direct routing choices, it still typically involves navigating through specific waypoints, including designated entry and exit points of an airspace.

The proposed method can accommodate such operational aspects by performing certain modifications to the problem formulation. For instance, a penalization mechanism can be incorporated into our optimization model to avoid frequent flight

<sup>4</sup> <https://www.sesarju.eu/projects/CICONIA>

Optimization of Top 50 routes on December 20, 2018 (1200UTC)

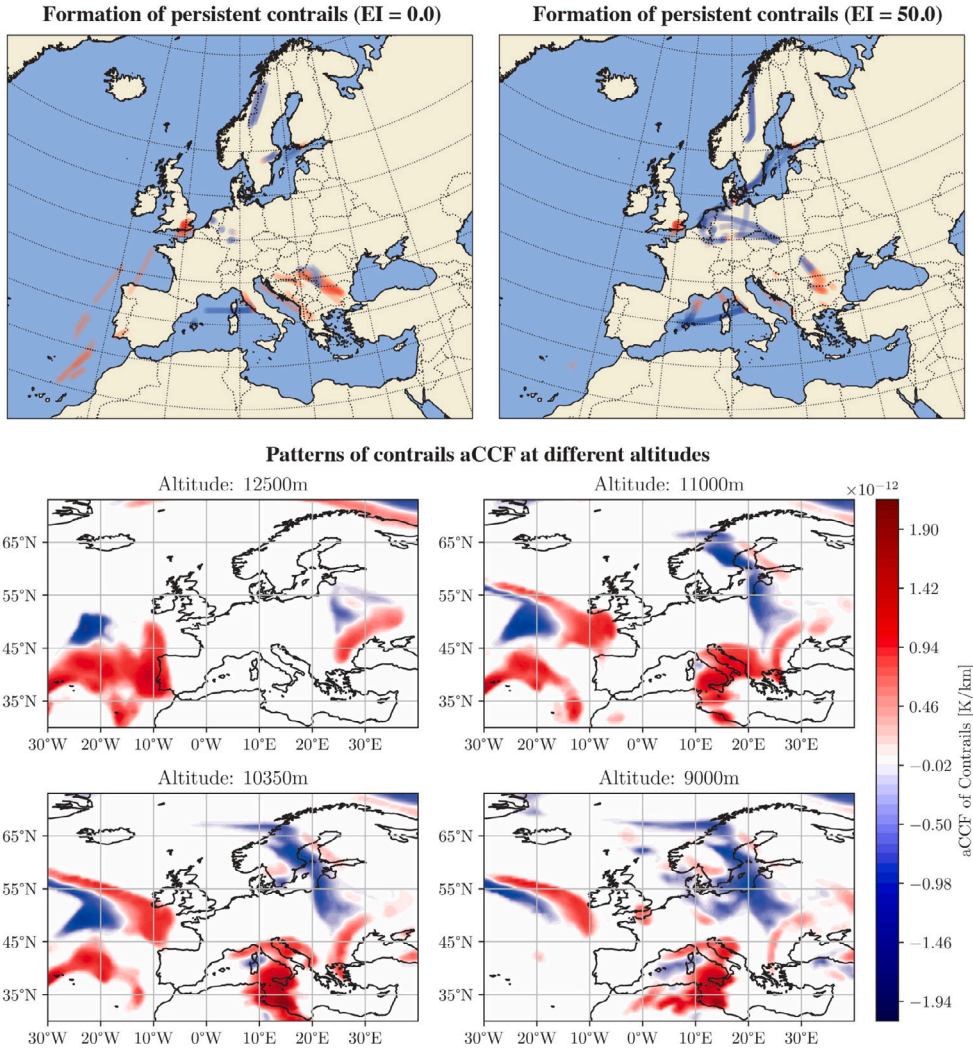


Fig. 15. Formation of persistent contrails (cooling (●)/warming (●)) along the flight path for the optimized top 50 routes on December 20, 2018 (1200UTC).

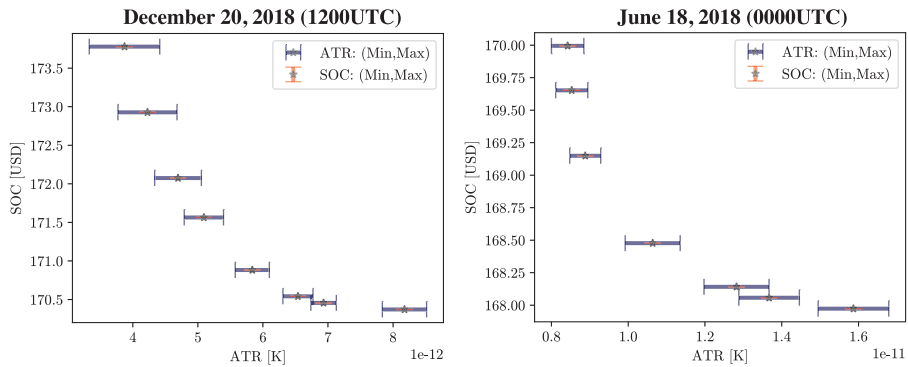


Fig. 16. Pareto-frontiers generated by varying the weighting parameter penalizing average climate effects, i.e., EI, for the optimization of the top 50 routes.

level changes that could impact passenger comfort. i.e., including the rate of altitude change in the cost functional of the optimization problem, as shown below:

$$J = \dots + R_h \int_0^{s_f} \dot{h}^2(s) ds$$

where  $R_h$  [USD. $s^2/m^2$ ] is a weighting parameter, penalizing the rate of altitude change. Higher values for  $R_h$  lead to smoother altitude profiles. By employing a distance-dependent weight (i.e.,  $R_h(s)$ ), the penalization can be differentiated between the climb/descent and cruise phases, which should be applied through a sigmoid function (i.e., smoothed version of a sign function). Such an approach provides flexibility in optimizing flight altitude based on the desired criteria, e.g., aligning closely with those currently being executed, thereby maintaining passenger comfort. The same cost-functional-based approach can be used to consider waypoints within the proposed framework. The distance from the waypoints should be penalized in the cost functional of the optimal control problem with distance-dependent weights, which are activated at specific points only once along the trajectory (i.e., one point for each waypoint). These points should be considered as additional decision variables within the optimization problem to be optimized. It is worth mentioning that a more general approach is to divide the formulated optimization problem into several sub-problems, each for each pair of waypoints, called multi-phase optimal control problem (Ross and Fahroo, 2004). With such an approach, the trajectory continuity due to transition should be penalized as additional constraints.

- The proposed flight planning framework is conceptualized as a flight dispatching solution. Consequently, in terms of implementation procedure, it should follow the established protocols and operational workflows that are currently in place for flight planning and management within the aviation industry. However, it is important to note that the proposed method is forward-looking and specifically geared toward a fully free-routing airspace. This future-oriented design means the proposed method is designed to handle more flexible and dynamic routing options, which may not be fully compatible with the highly structured and static nature of today's ATM infrastructure. Despite this, the core aspect of the developed methodology – the integration of uncertainty into the flight planning process to generate a deterministic and robust climate-optimized flight plan (achieved through robust tracking problem formulation) – is generic. Thus, the introduced framework is not limited to the context of unconstrained airspace explored in this study and can be adapted to the existing operational flight planning tools.

## 6. Conclusion

This paper addressed the full 4D robust aircraft trajectory optimization problem considering aviation-induced climate effects and meteorological uncertainty. The climate-sensitive areas were determined utilizing aCCFs V1.0 A. We used the EPS to quantify uncertainty in meteorological variables and, consequently, uncertainties in the calculated aCCFs. We observed a considerable level of uncertainty in the contrails aCCF primarily because of the significant variability among the ensemble members of relative humidity retrieved from the EPS. To address meteorological uncertainty in path planning, a robust aircraft trajectory optimization was formulated within the context of optimal control theory. The performance index was selected in a manner to allow for simultaneous control over both the average and dispersion of operating costs and climate effects. The effectiveness of the proposed methodology in dealing with meteorological uncertainty was supported by studying three different scenarios. It was concluded that despite being highly uncertain, the average mitigation potential is higher when there is a possibility of forming persistent contrails. During the night-time, the uncertainty ranges were also reduced by penalizing the average climate effects, whereas, during the daytime, the variance of the climate effects had to be penalized for lowering uncertainty effects. We concluded that it was possible to determine a cost-effective climate-optimized trajectory with minimal sensitivity to meteorological uncertainty by selecting appropriate weights for the objectives in the defined cost functional.

### Code availability

The robust flight planning method introduced in this paper has been made available as an open-source Python library named ROC (Robust Optimal Control for flight planning). ROC is released under the GNU Lesser General Public License (Version 3.0). The development version can be found at <https://github.com/Aircraft-Operations-Lab/roc>, and the first release is available via the DOI: <https://doi.org/10.5281/zenodo.10552812>.

### CRedit authorship contribution statement

**Abolfazl Simorgh:** Writing – review & editing, Writing – original draft, Visualization, Software, Methodology, Conceptualization. **Manuel Soler:** Methodology, Conceptualization, Supervision, Writing – original draft, Writing – review & editing. **Simone Dietmüller:** Writing – review & editing, Methodology, Data curation. **Sigrun Matthes:** Writing – review & editing, Funding acquisition, Conceptualization. **Hiroshi Yamashita:** Writing – review & editing, Data curation. **Federica Castino:** Writing – review & editing, Data curation. **Feijia Yin:** Writing – review & editing, Writing – original draft, Conceptualization.

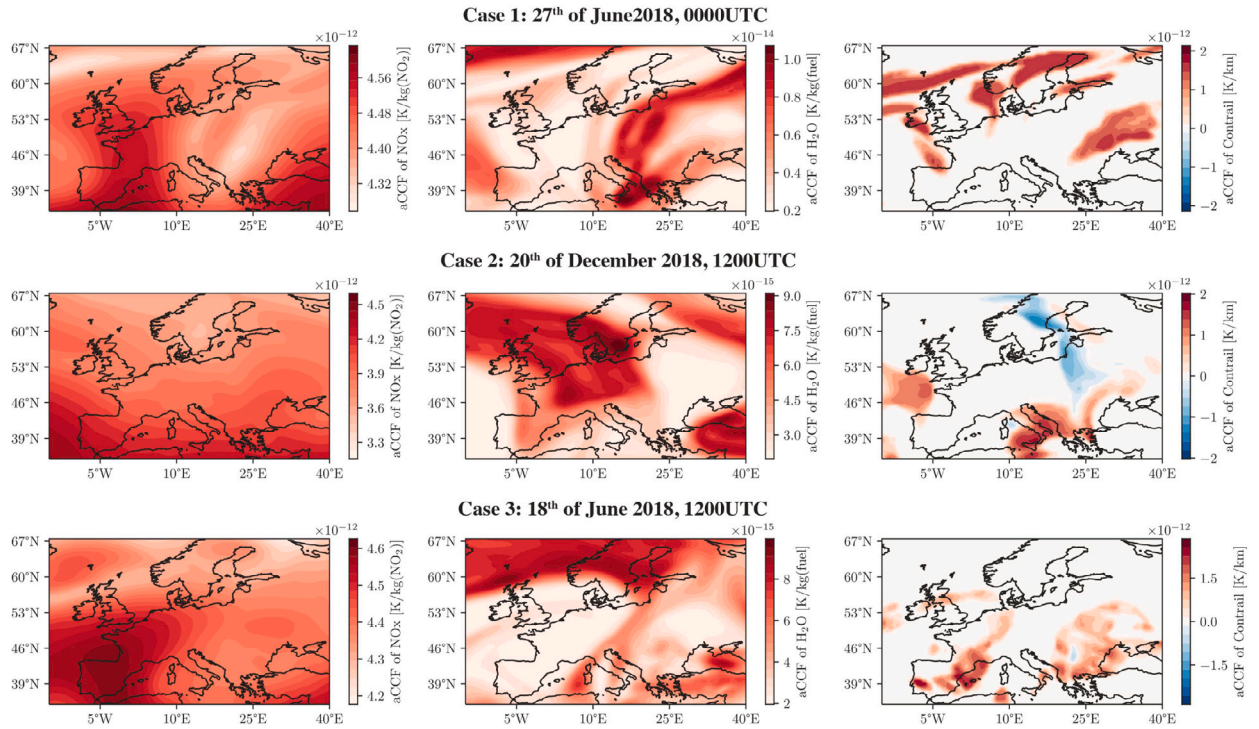


Fig. 17. Patterns of aCCFs at pressure level 250 hPa ( $\approx 11$  km) for three considered scenarios.

## Financial support

This research was carried out as a part of EU-projects FlyATM4E and RefMAP. FlyATM4E has received funding from the SESAR Joint Undertaking (JU) under the European Union's Horizon 2020 research and innovation programme under grant agreement No 891317. The JU receives support from the European Union's Horizon 2020 research and innovation programme and the SESAR JU members other than the Union. RefMAP has received funding from the Horizon Europe programme 2023 under grant agreement No 101096698. The opinions expressed herein reflect the authors' views only. Under no circumstances shall the Horizon Europe programme be responsible for any use that may be made of the information contained herein.

## Appendix A. Patterns of aCCFs

The patterns of aCCFs for the three considered cases are illustrated in Fig. 17, showing strong variability to the meteorological conditions.

## Appendix B. PCFAs for an ensemble weather forecast

Areas suitable to form persistent contrails are depicted in Fig. 18 for nine different members of an ERA5 weather data. High variability between ensemble members can be observed.

## Appendix C. Comparison of proposed robust flight planning versus a deterministic approach

For a flight from Belgrade to Luxembourg on the 13th of June 2018, departing at 0000UTC, we solve the following optimization problems: (1) (robust) cost-optimal flight planning problem, (2) 10 deterministic climate-optimal flight planning problems, each associated with one ensemble member provided by the ERA5 data products and (3) the proposed robust optimization problem incorporating all ensemble members. To formulate deterministic optimization problems, we consider only one of the ensemble members when building the augmented dynamical model (see Section 4.1), i.e.,  $N_{\text{EPS}} = 1$ . The assessments of climate impacts, as depicted in Fig. 19, reveal that deterministic optimizations effectively mitigate the climate effects estimated using the ensemble member selected for the trajectory optimization. This can be clearly seen by treating the figure as a matrix (while excluding the columns related to the proposed robust approach and the cost-optimal scenario), where the diagonal elements, showing both the optimization and assessment based on the same ensemble member, represent the minimum values observed. However, these trajectories do not necessarily mitigate climate effects when evaluated based on other ensemble members not considered for

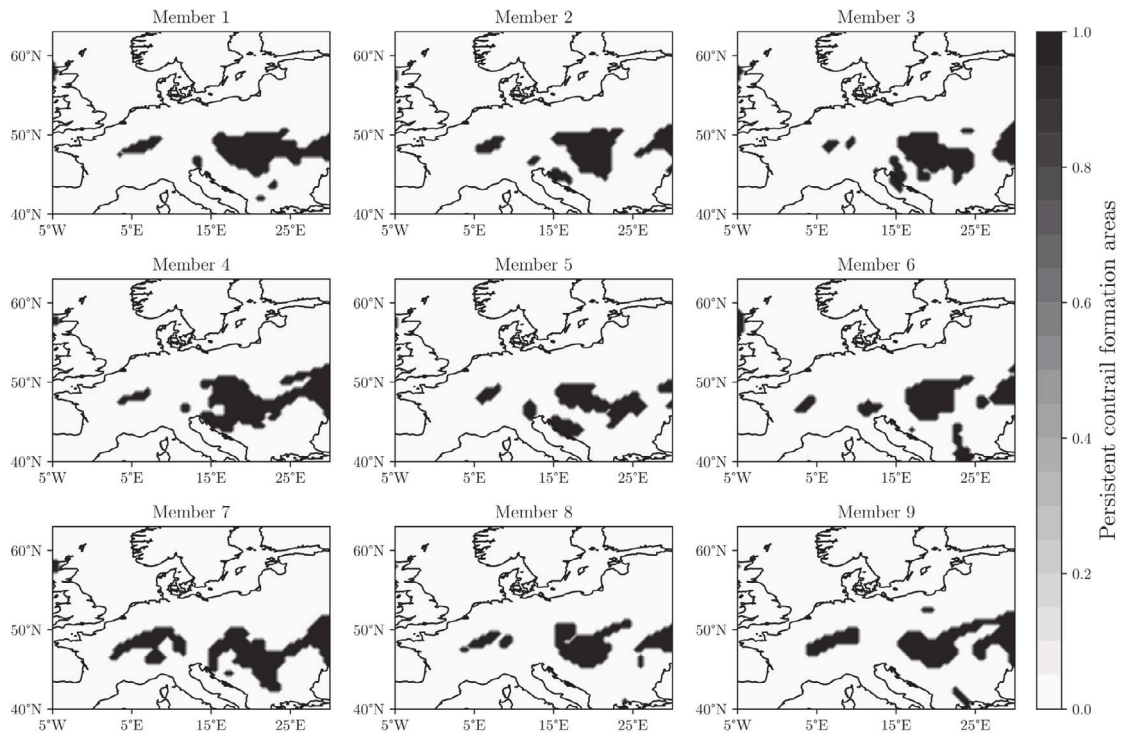


Fig. 18. PCFAs calculated using different ensemble members (i.e., nine different members of an ERA5 ensemble data product) at 225 hPa on June 13, 2018, 0000 UTC.

optimization, indicating a lack of robustness. In contrast, the proposed approach mitigates the climate impact consistently across all ten potential assessments, thereby demonstrating its robust performance.

To delve deeper into the results, we perform optimizations using only three ensemble members (i.e., ensemble members 2, 3, and 4). The climate impact assessments and flight altitudes are presented in Fig. 20, and the lateral paths with the aCCF of contrails are depicted in Fig. 21. By relating the flight altitudes in Fig. 20-b to the corresponding aCCF of contrails given in Fig. 21, we observe that in deterministic scenarios, as expected, the optimizer tends to avoid the formation of warming contrails for the ensemble member considered in the optimization. This strategy, however, may result in generating persistent contrails when assessed based on other members. Looking at the flight altitude associated with the proposed robust approach (dashed line in Fig. 20-b), one can see that from the start of the flight up to 250 NM, it is similar to the altitude profile obtained from the deterministic optimization concerning ensemble member 3. From 250 NM to 500 NM, it follows the deterministic optimization for ensemble member 2, and from 500 NM toward the end of the flight, it resembles the deterministic optimization for ensemble member 4. Such altitude profile avoids forming persistent contrails with all three potential weather scenarios (see Fig. 21), ensuring robust performance.

#### Appendix D. Comparison of trajectories optimized within free-routing and structured airspace

In this section, the flight planning method developed for a fully free-routing airspace in this study is compared with the method we proposed for structured airspace in Simorgh et al. (2023), which is also able to incorporate meteorological uncertainty in planning climate-optimized aircraft trajectories. An open-source Python library called ROOST<sup>5</sup> was developed for the optimization method proposed in Simorgh et al. (2023) which can be accessed using DOI: <https://doi.org/10.5281/zenodo.7495472>. Hereafter, we refer to the optimization methods for free-routing and structured airspace as ROC and ROOST, respectively. For the comparison, we have focused on two routing options: cost-optimal and climate-optimal. The results are presented in Figs. (22, 23) and are summarized in (Table D.5). When optimizing for operating cost, the optimizer within the free-routing context (i.e., ROC) tends to select more direct routes compared to ROOST, which is constrained by specific airways and waypoints. Such flexibility in route selection led to a 6% reduction in the operating cost. In the climate-optimal routing scenario, the free-routing optimizer deviates effectively from the shortest path to maximize the generation of cooling contrails, achieving a 36% reduction in climate impact and a 3.8% reduction in the operating cost compared to the similar routing strategy with ROOST. This comparison highlights the advantages of increased flexibility in route selection, thus reinforcing the motivation for the research.

<sup>5</sup> <https://github.com/Aircraft-Operations-Lab/roost>

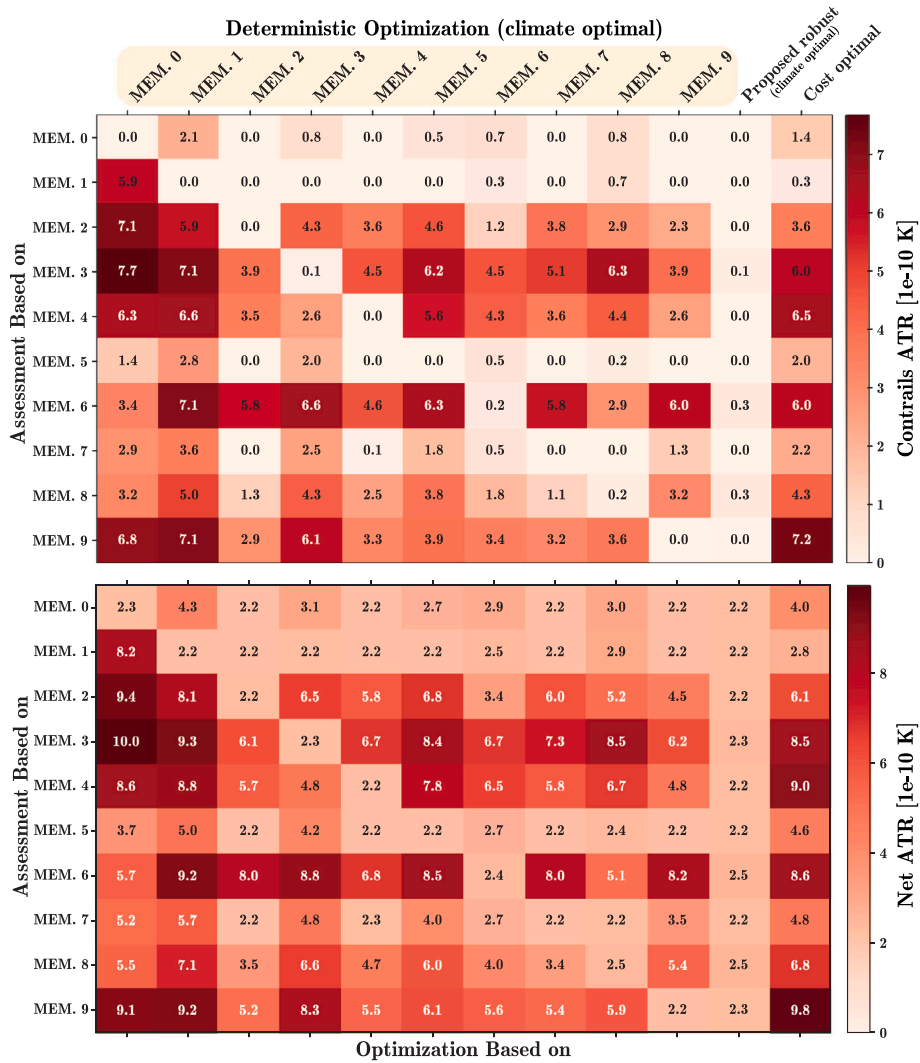


Fig. 19. Assessment of climate impact (of contrails and all non-CO<sub>2</sub> species) for different optimization scenarios: deterministic climate-optimized flight planning, proposed robust climate-optimized flight planning, and cost-optimized flight planning.

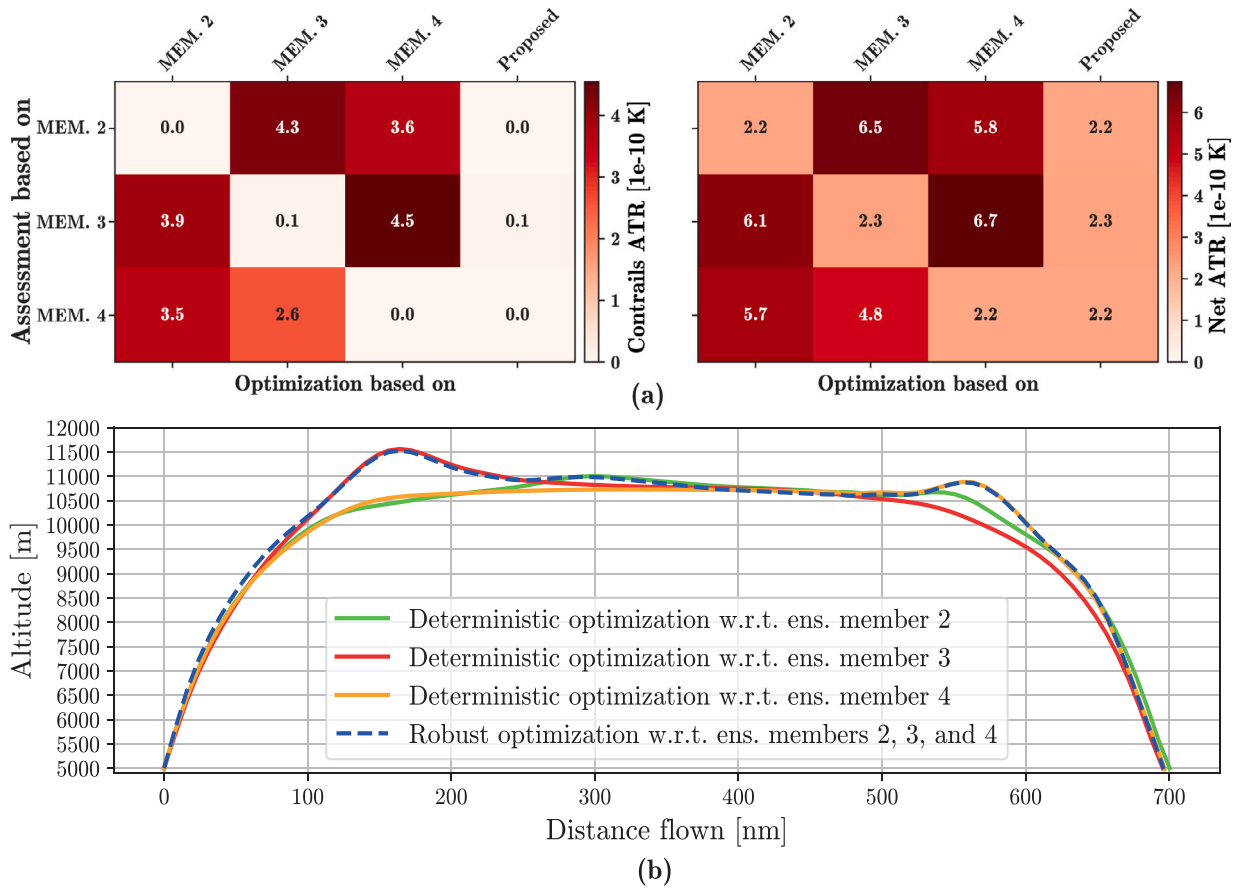


Fig. 20. (a) Assessment of climate impact (of contrails and all non-CO<sub>2</sub> species) and (b) flight altitudes for different optimization scenarios: deterministic climate-optimized flight planning and proposed robust climate-optimized flight planning.

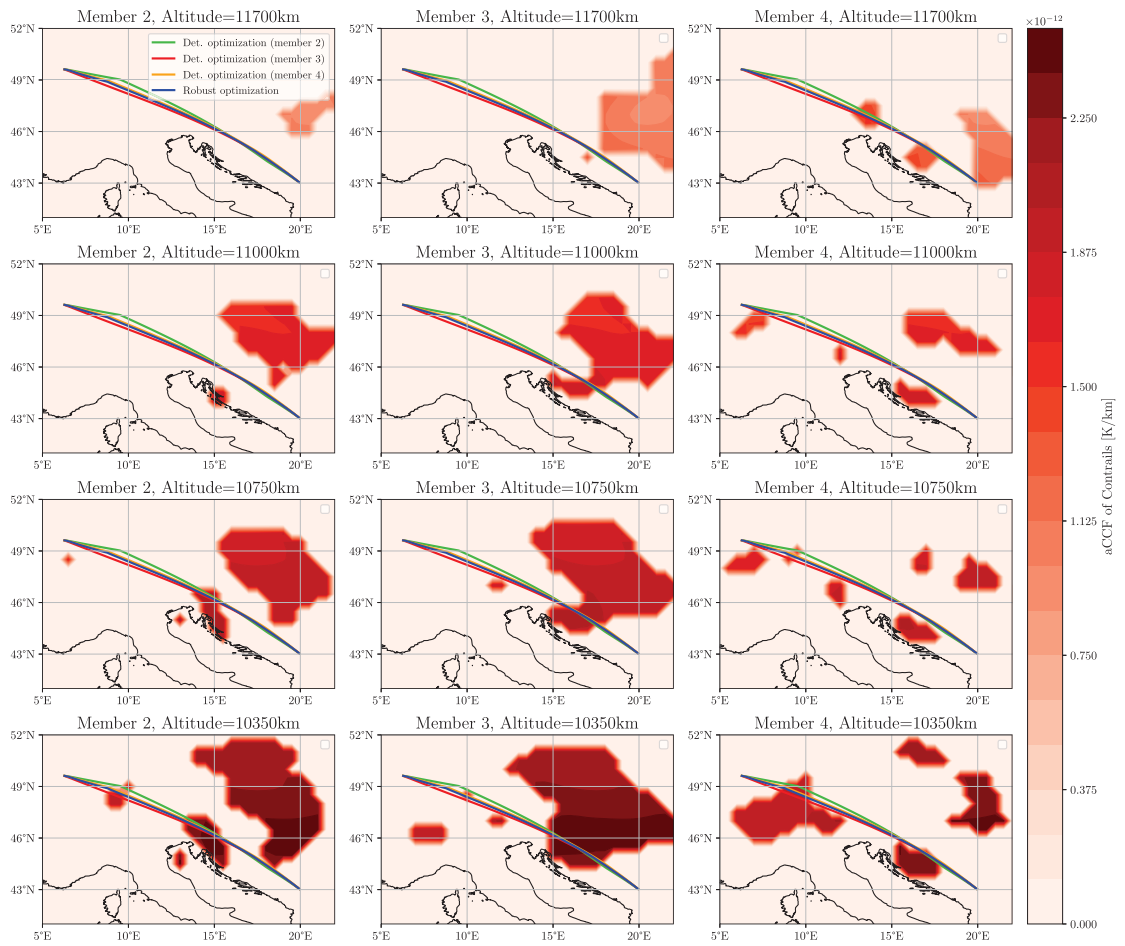


Fig. 21. Lateral paths with the aCCF of contrails for different optimization scenarios.

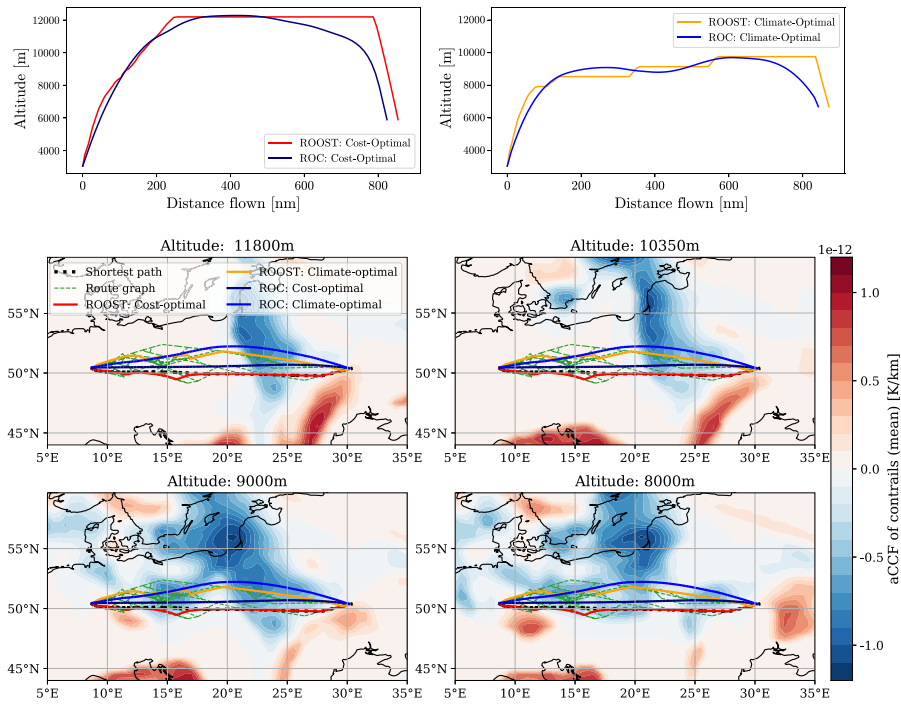


Fig. 22. Comparison of ROOST (structured) and ROC (free-routing) optimizers: Flight altitudes and lateral paths.

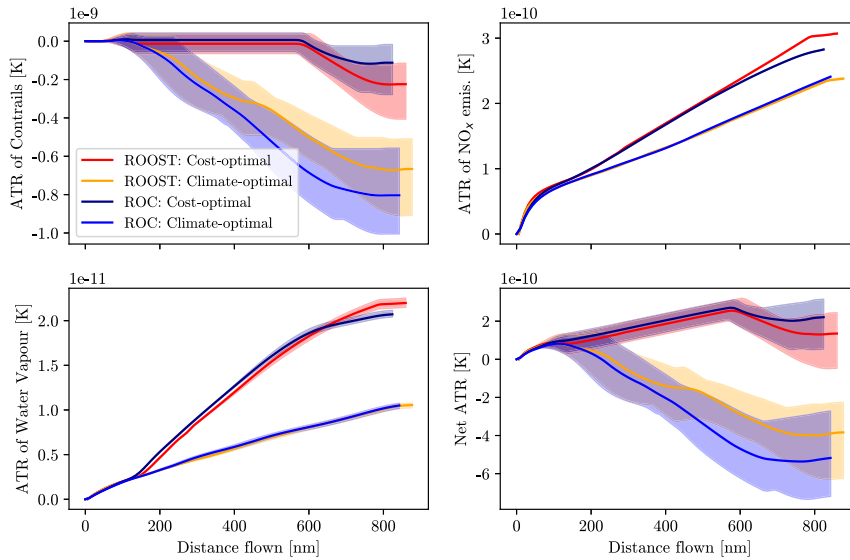


Fig. 23. Comparison of ROOST (structured) and ROC (free-routing) optimizers: Climate impact.

Table D.5  
Comparison of ROOST and ROC optimizers: performance variables.

Performance variables	ROOST: Cost-optimal	ROOST: Climate-optimal	ROC: Cost-optimal	ROC: Climate-optimal
Flight time [min.]	113.5	116.7	106.1	110.3
Fuel consumption [kg]	4412.9	4954.6	4183.2	4933.0
Operating cost [USD]	7360.7	7778.2	6911.0	7483.1
ATR [K]	1.3e-10	-3.8e-10	2.15e-10	-5.17e-10

## References

- Appleman, H., 1953. The formation of exhaust condensation trails by jet aircraft. *Bull. Am. Meteorol. Soc.* 34 (1), 14–20.
- Baneshi, F., Soler, M., Simorgh, A., 2023. Conflict assessment and resolution of climate-optimal aircraft trajectories at network scale. *Transp. Res. D* 115, 103592.
- Bauer, P., Thorpe, A., Brunet, G., 2015. The quiet revolution of numerical weather prediction. *Nature* 525 (7567), 47–55.
- Betts, J.T., 2010. *Practical Methods for Optimal Control and Estimation Using Nonlinear Programming*. SIAM.
- Brasseur, G.P., Gupta, M., Anderson, B.E., Balasubramanian, S., Barrett, S., Duda, D., Fleming, G., Forster, P.M., Fuglestedt, J., Gettelman, A., et al., 2016. Impact of aviation on climate: FAA's aviation climate change research initiative (ACCRI) phase II. *Bull. Am. Meteorol. Soc.* 97 (4), 561–583.
- Campbell, S., Neogi, N., Bragg, M., 2008. An optimal strategy for persistent contrail avoidance. In: *AIAA Guidance, Navigation and Control Conference and Exhibit*. p. 6515.
- Castino, F., Yin, F., Grewe, V., Yamashita, H., Matthes, S., Dietmüller, S., Baumann, S., Soler, M., Simorgh, A., Mendiguchia Meuser, M., Linke, F., Lührs, B., 2023. Decision-making strategies implemented in SolFinder 1.0 to identify eco-efficient aircraft trajectories: application study in AirTraF 3.0. *Geosci. Model Dev. Discuss.* 2023, 1–31. URL: <https://gmd.copernicus.org/preprints/gmd-2023-88/>.
- Celis, C., Sethi, V., Zammit-Mangion, D., Singh, R., Piliadis, P., 2014. Theoretical optimal trajectories for reducing the environmental impact of commercial aircraft operations. *J. Aerosp. Technol. Manag.* 6 (1), 29–42.
- Dahlmann, K., Grewe, V., Frömming, C., Burkhardt, U., 2016. Can we reliably assess climate mitigation options for air traffic scenarios despite large uncertainties in atmospheric processes? *Transp. Res. D* 46, 40–55.
- Debusschere, B.J., Najm, H.N., Pébay, P.P., Knio, O.M., Ghanem, R.G., Le Maître, O.P., 2004. Numerical challenges in the use of polynomial chaos representations for stochastic processes. *SIAM J. Sci. Comput.* 26 (2), 698–719.
- Dietmüller, S., Matthes, S., Dahlmann, K., Yamashita, H., Simorgh, A., Soler, M., Linke, F., Lührs, B., Meuser, M.M., Weder, C., Grewe, V., Yin, F., Castino, F., 2023. A python library for computing individual and merged non-CO<sub>2</sub> algorithmic climate change functions: CLIMaCCF V1.0. *Geosci. Model Dev.* 16 (15), 4405–4425.
- DuBois, D., Paynter, G.C., 2006. “Fuel Flow Method 2” for estimating aircraft emissions. *SAE Trans.* 1–14.
- EUROCONTROL, 2022. *Eurocontrol aviation outlook 2050*. URL: <https://www.eurocontrol.int/publication/eurocontrol-aviation-outlook-2050>.
- Gallo, E., Navarro, F., Nuic, A., Igaru, M., 2006. Advanced aircraft performance modeling for ATM: BADA 4.0 results. In: *2006 Ieee/Aiaa 25TH Digital Avionics Systems Conference*. IEEE, pp. 1–12.
- Gierens, K., Matthes, S., Rohs, S., 2020. How well can persistent contrails be predicted? *Aerospace* 7 (12), 169.
- González-Arribas, D., Baneshi, F., Andrés, E., Soler, M., Jardines, A., Garcia-Heras, J., 2023. Fast 4D flight planning under uncertainty through parallel stochastic path simulation. *Transp. Res. C* 148, 104018. URL: <https://www.sciencedirect.com/science/article/pii/S0968090X23000074>.
- González-Arribas, D., Soler, M., Sanjurjo-Rivo, M., 2018. Robust aircraft trajectory planning under wind uncertainty using optimal control. *J. Guid. Control Dyn.* 41 (3), 673–688.
- Hartjes, S., Hendriks, T., Visser, D., 2016. Contrail mitigation through 3D aircraft trajectory optimization. In: *16th AIAA Aviation Technology, Integration, and Operations Conference*. p. 3908.
- Hersbach, H., Bell, B., Berrisford, P., Hirahara, S., Horányi, A., Muñoz-Sabater, J., Nicolas, J., Peubey, C., Radu, R., Schepers, D., et al., 2020. The ERA5 global reanalysis. *Q. J. R. Meteorol. Soc.* 146 (730), 1999–2049.
- International Air Transport Association (IATA), 2022. *Air passenger numbers to recover in 2024*. URL: <https://www.iata.org/en/pressroom/2022-releases/2022-03-01-01/>.
- Kirk, D.E., 2004. *Optimal Control Theory: An Introduction*. Courier Corporation.
- Lee, D.S., Fahey, D.W., Forster, P.M., Newton, P.J., Wit, R.C., Lim, L.L., Owen, B., Sausen, R., 2009. Aviation and global climate change in the 21st century. *Atmos. Environ.* 43 (22–23), 3520–3537.
- Lee, D.S., Fahey, D., Skowron, A., Allen, M., Burkhardt, U., Chen, Q., Doherty, S., Freeman, S., Forster, P., Fuglestedt, J., et al., 2021. The contribution of global aviation to anthropogenic climate forcing for 2000 to 2018. *Atmos. Environ.* 244, 117834.
- Lee, D.S., Pitari, G., Grewe, V., Gierens, K., Penner, J.E., Petzold, A., Prather, M., Schumann, U., Bais, A., Bernsten, T., et al., 2010. Transport impacts on atmosphere and climate: Aviation. *Atmos. Environ.* 44 (37), 4678–4734.
- Lim, Y., Gardi, A., Sabatini, R., 2017. Optimal aircraft trajectories to minimize the radiative impact of contrails and CO<sub>2</sub>. *Energy Procedia* 110, 446–452.
- Lührs, B., Linke, F., Matthes, S., Grewe, V., Yin, F., 2021. Climate impact mitigation potential of European air traffic in a weather situation with strong contrail formation. *Aerospace* 8 (2), 50.
- Lührs, B., Niklass, M., Froemming, C., Grewe, V., Gollnick, V., 2016. Cost-benefit assessment of 2D and 3D climate and weather optimized trajectories. In: *16th AIAA Aviation Technology, Integration, and Operations Conference*. p. 3758.
- Matthes, S., Dietmüller, S., Dahlmann, K., Frömming, C., Peter, P., Yamashita, H., Grewe, V., Yin, F., Castino, F., 2023. Updated algorithmic climate change functions (aCCF) V1. 0A: evaluation with the climate-response model AirClim V2. 0. *Geosci. Model Dev. Discuss.* 2023, 1–28.
- Matthes, S., Grewe, V., Dahlmann, K., Frömming, C., Irvine, E., Lim, L., Linke, F., Lührs, B., Owen, B., Shine, K., et al., 2017. A concept for multi-criteria environmental assessment of aircraft trajectories. *Aerospace* 4 (3), 42.
- Mendiguchia Meuser, M., Lührs, B., Gollnick, V., Linke, F., Matthes, S., Dietmüller, S., Baumann, S., Soler, M., Simorgh, A., Yin, F., et al., 2022. Mitigation of aviation's climate impact through robust climate optimized trajectories in intra-european airspace. In: *33th Congress of the International Council of the Aeronautical Sciences Stockholm, Sweden*.
- Niklaß, M., Gollnick, V., Lührs, B., Dahlmann, K., Froemming, C., Grewe, V., van Manen, J., 2017. Cost-benefit assessment of climate-restricted airspaces as an interim climate mitigation option. *J. Air Transp.* 25 (2), 27–38.
- Niklaß, M., Grewe, V., Gollnick, V., Dahlmann, K., 2021. Concept of climate-charged airspaces: a potential policy instrument for internalizing aviation's climate impact of non-CO<sub>2</sub> effects. *Climate Policy* 21 (8), 1066–1085.
- Reutter, P., Neis, P., Rohs, S., Sauvage, B., 2020. Ice supersaturated regions: Properties and validation of ERA-Interim reanalysis with IAGOS in situ water vapour measurements. *Atmos. Chem. Phys.* 20 (2), 787–804.
- Rosenow, J., Lindner, M., Fricke, H., 2017. Impact of climate costs on airline network and trajectory optimization: A parametric study. *CEAS Aeronaut. J.* 8 (2), 371–384.
- Ross, I.M., Fahroo, F., 2004. Pseudospectral knotting methods for solving nonsmooth optimal control problems. *J. Guid. Control Dyn.* 27 (3), 397–405.
- Schumann, U., 2012. A contrail cirrus prediction model. *Geosci. Model Dev.* 5 (3), 543–580.
- Schumann, U., Graf, K., Mannstein, H., 2011. Potential to reduce the climate impact of aviation by flight level changes. In: *3rd AIAA Atmospheric Space Environments Conference*. p. 3376.
- Schumann, U., Poll, I., Teoh, R., Koelle, R., Spinielli, E., Molloy, J., Koudis, G.S., Baumann, R., Bugliaro, L., Stettler, M., et al., 2021. Air traffic and contrail changes over Europe during COVID-19: A model study. *Atmos. Chem. Phys.* 21 (10), 7429–7450.
- Shapiro, M., Engberg, Z., Zucig, B., Teoh, R., Stettler, M., Schumann, U., McKay, I., 2022. Forecasting contrail climate forcing for flight planning and air traffic management applications. In: *The 5<sup>th</sup> International Conference on Transport, Atmosphere and Climate*. TAC.
- Simorgh, A., Soler, M., 2022. Non-CO<sub>2</sub> market-based incentives towards robust climate optimal aircraft trajectories. In: *Proceedings of International Workshop on ATM/CNS*, vol. 1, pp. 156–163.

- Simorgh, A., Soler, M., González-Arribas, D., 2022. Robust climate optimal aircraft trajectory planning considering uncertainty in weather forecast. In: Proceedings of the 2022 CEAS EuroGNC Conference. Berlin, Germany, CEAS-GNC-2022-043.
- Simorgh, A., Soler, M., González-Arribas, D., Linke, F., Lührs, B., Meuser, M.M., Dietmüller, S., Matthes, S., Yamashita, H., Yin, F., et al., 2023. Robust 4D climate-optimal flight planning in structured airspace using parallelized simulation on GPUs: ROOST V1.0. *Geosci. Model Dev.* 16 (13), 3723–3748.
- Simorgh, A., Soler, M., González-Arribas, et al., 2022b. A comprehensive survey on climate optimal aircraft trajectory planning. *Aerospace* 9 (3), 146.
- Single European Sky ATM Research Joint Undertaking (SESAR JU), 2020. European ATM Master Plan: Executive View. Publications Office.
- Soler, M., Zou, B., Hansen, M., 2014. Flight trajectory design in the presence of contrails: Application of a multiphase mixed-integer optimal control approach. *Transp. Res. C* 48, 172–194.
- Sridhar, B., Ng, H.K., Chen, N.Y., 2011. Aircraft trajectory optimization and contrails avoidance in the presence of winds. *J. Guid. Control Dyn.* 34 (5), 1577–1584.
- Wächter, A., Biegler, L.T., 2006. On the implementation of an interior-point filter line-search algorithm for large-scale nonlinear programming. *Math. Program.* 106 (1), 25–57.
- Yamashita, H., Yin, F., Grewe, V., Jöckel, P., Matthes, S., Kern, B., Dahlmann, K., Frömming, C., 2020. Newly developed aircraft routing options for air traffic simulation in the chemistry–climate model EMAC 2.53: AirTraf 2.0. *Geosci. Model Dev.* 13 (10), 4869–4890.
- Yamashita, H., Yin, F., Grewe, V., Jöckel, P., Matthes, S., Kern, B., Dahlmann, K., Frömming, C., 2021. Analysis of aircraft routing strategies for North Atlantic flights by using AirTraf 2.0. *Aerospace* 8 (2), 33.
- Yin, F., Grewe, V., Castino, F., Rao, P., Matthes, S., Dahlmann, K., Dietmüller, S., Frömming, C., Yamashita, H., Peter, P., et al., 2023. Predicting the climate impact of aviation for en-route emissions: The algorithmic climate change function submodel ACCF 1.0 of EMAC 2.53. *Geosci. Model Dev.* 16 (11), 3313–3334.